

Vision paper

## Hydraulics of aerated flows: *qui pro quo?*

HUBERT CHANSON (IAHR Member), Professor, *School of Civil Engineering, The University of Queensland, Brisbane, Australia*  
Email: [h.chanson@uq.edu.au](mailto:h.chanson@uq.edu.au) (author for correspondence)

### ABSTRACT

In turbulent free-surface flows, the deformation of the surface leads to air bubble entrainment and droplet projections when the turbulent shear stress is greater than the surface tension stress that resists to the interfacial breakup. These complex processes at the water–air interface have been the focus of extensive experimental, numerical and theoretical studies over last two decades and this paper reviews the key advancements. It is highlighted that the recent progress in metrology enables the detailed measurements of a range of air–water flow properties under controlled flow conditions, representing the *sine qua non* requirement for the development of improved physical understanding and for validating phenomenological and numerical models. The author believes that the future research into aerated flow hydraulics should focus on field measurements of high quality, development of new measurement approaches and data analyses tools, computational fluid dynamics modelling of aerated flows, and the mechanics of aerated flows in conduits.

**Keywords:** Air–water flows; air entrainment; dynamic similarity; hydraulic modelling; metrology; multiphase flows

### 1 Introduction

In high-velocity free-surface flows, large quantities of air are exchanged at the free-surfaces and the air–water flow becomes a compressible fluid with density  $\rho_w(1 - C) + \rho_a C \approx \rho_w(1 - C)$ , where  $\rho_w$  is the water density,  $\rho_a$  is the air density and  $C$  is the void fraction. Such flows are encountered in a wide range of applications in chemical, civil, environmental, mechanical, mining and nuclear engineering. In hydraulic engineering, the flow aeration may induce some flow bulking (Falvey 1980, Wood 1985, 1991, Brocchini and Peregrine 2001b) and turbulence modulation which might lead to some drag reduction or enhanced turbulent kinetic energy dissipation depending on the flow characteristics. Drag reduction in aerated flows was documented for chute spillways (Jevdjevich and Levin 1953, Wood 1983, Chanson 1994, 2004a) as well as for high-speed submerged bodies with micro-bubble injection (Bogdevich *et al.* 1977, Madavan *et al.* 1984, Marié 1987). The aeration of the flow may enhance the rate of energy dissipation in plunging breaking waves (Führboter 1970, Chanson and Lee 1997, Hoque and Aoki 2005a), and reduce the breakup length of water jets discharging into atmosphere (Héraud 1966, Ervine and Falvey 1987, Augier 1996). The air entrainment may also prevent or lessen the damage caused by cavitation (Peterka 1953, Russell and Sheehan 1974, Falvey 1990). In relation to environmental processes, it does substantially contribute to the air–water mass transfer of

atmospheric gases (Wilhelms and Gulliver 1989, Gulliver 1990, Toombes and Chanson 2005). Altogether, it is acknowledged that design engineers must take into account the effects of flow aeration: “*Consideration of the effects of entrained air upon water flow may be essential to provide for the safe operation of a hydraulic structure*” (Wood 1991); “*Self-aeration is by far the most important feature of supercritical flow*” (Novak *et al.* 2001).

Since the first successful experiments by Ehrenberger (1926), some major contributions included Straub and Anderson (1958) for supercritical flows, Rajaratnam (1962) and Resch and Leutheusser (1972) for hydraulic jumps, Hoyt and Taylor (1977) for high-speed water jets, Ervine *et al.* (1980) for plunging jets. Although there have been several experimental studies over the recent decades (see reviews in Wood 1991, Chanson 1997a), there have been only a few detailed field measurements. Among these are milestone studies at the Aviemore dam spillway (Keller 1972, Cain 1978, Cain and Wood 1981a,b) and near-full-scale laboratory experiments of Arreguin and Echavez (1986), Xi (1988) and Chanson (2007a). Importantly, all the experimental investigations highlighted the strong interactions between entrained bubbles and turbulence (Brocchini and Peregrine 2001a,b, Hanratty *et al.* 2003, Balachandar and Eaton 2010). Despite a number of significant advances (Rao and Kobus 1971, Wood 1991, Chanson 1997a, Brocchini and Peregrine 2001b), there are some fundamental issues related to the modelling of aerated flows, turbulence modulation by air bubbles and

Revision received 3 June 2013/Open for discussion until 30 November 2013.

extrapolation of laboratory and numerical results to full-scale prototype structures (Ervine 1998). There are significant needs for detailed field measurements. In this paper, a brief review of aerated flows is first presented. Then, the basic equations and latest advances in the modelling of aerated flows are identified, and the metrology of air–water flows in hydraulic engineering is discussed. The findings emphasize the complexity of the aeration process and address some misunderstandings (*qui pro quo*). A vision for future research developments concludes the paper.

### 1.1 Aerated flows in hydraulic engineering

Aerated flows are often observed in low-, medium- and high-head structures, including storm waterways, culverts, dropshafts, spillway chutes, water jets taking off from flip bucket and stilling basins. Figures 1 and 2 illustrate some typical hydraulic engineering applications. Aerated flows are observed in small-scale as well as large-scale flows: from a water jet in a fountain ( $Q_w \sim 10^{-3} \text{ m}^3/\text{s}$ ,  $d \sim 5 \text{ mm}$ ) to a large spillway during a major flood ( $Q_w > 50,000 \text{ m}^3/\text{s}$ ,  $d > 10 \text{ m}$ ), where  $Q_w$  is the water discharge and  $d$  is the flow thickness. In all cases, the interactions between the entrained air and the flow turbulence are very significant. In Fig. 1a–c, the maximum discharge capacity of the three dam spillways is about 65,000, 12,000 and 93,000  $\text{m}^3/\text{s}$ , respectively.

Most hydraulic engineering applications involve turbulent flows characterized by quasi-random unpredictable behaviour, strong mixing properties and a broad spectrum of velocity fluctuations (Bradshaw 1971, Tennekes and Lumley 1972). Aerated flows in hydraulic engineering are extremely complicated with a broad range of relevant length and time scales. The time scales range from less than 1 ms for the turbulence dissipation in a white-water stream to about 24 h and 50 min for the tidal cycle in coastal processes and to more than 50 years for the deep-sea oceanic currents controlling the balances between oxygen and carbon dioxide (Chanson 2004b, Bombardelli and Chanson 2009).

At the free-surface, the exchange of air and water is driven by the turbulence next to the air–water interface. The free-surface breakup and air entrainment occur when the turbulent shear stress is greater than the surface tension force per unit area resisting the interfacial breakup (Ervine and Falvey 1987, Chanson 2009). Once some air is entrained within the bulk of the flow, the break-up of air pockets occurs when the tangential shear stress is greater than the capillary force per unit area (Hinze 1955, Chanson 2009). As bubbles and droplets are advected by the flow, particle collisions may lead to their coalescence. The entire process is extremely complicated and experimental observations showed a broad range of air and water particle sizes in aerated flows (Halbronn *et al.* 1953, Thandaveswara 1974, Volkart 1980, Cummings and Chanson 1997b).



Figure 1 Aerated flows in hydraulic engineering. (a) The Burdekin Falls Dam (Australia) on 3 February 2007 (Courtesy of QLD Department of Environment and Mineral Resources and David Li), (b) the Wivenhoe dam spillway (Australia) on 17 January 2011, (c) the Paradise Dam spillway (Australia) on 30 December 2010 (Courtesy of Bernard Chanson) and (d) the flooding in Marburg (Australia) on 11 January 2011 (Courtesy of Nicole Chanson)

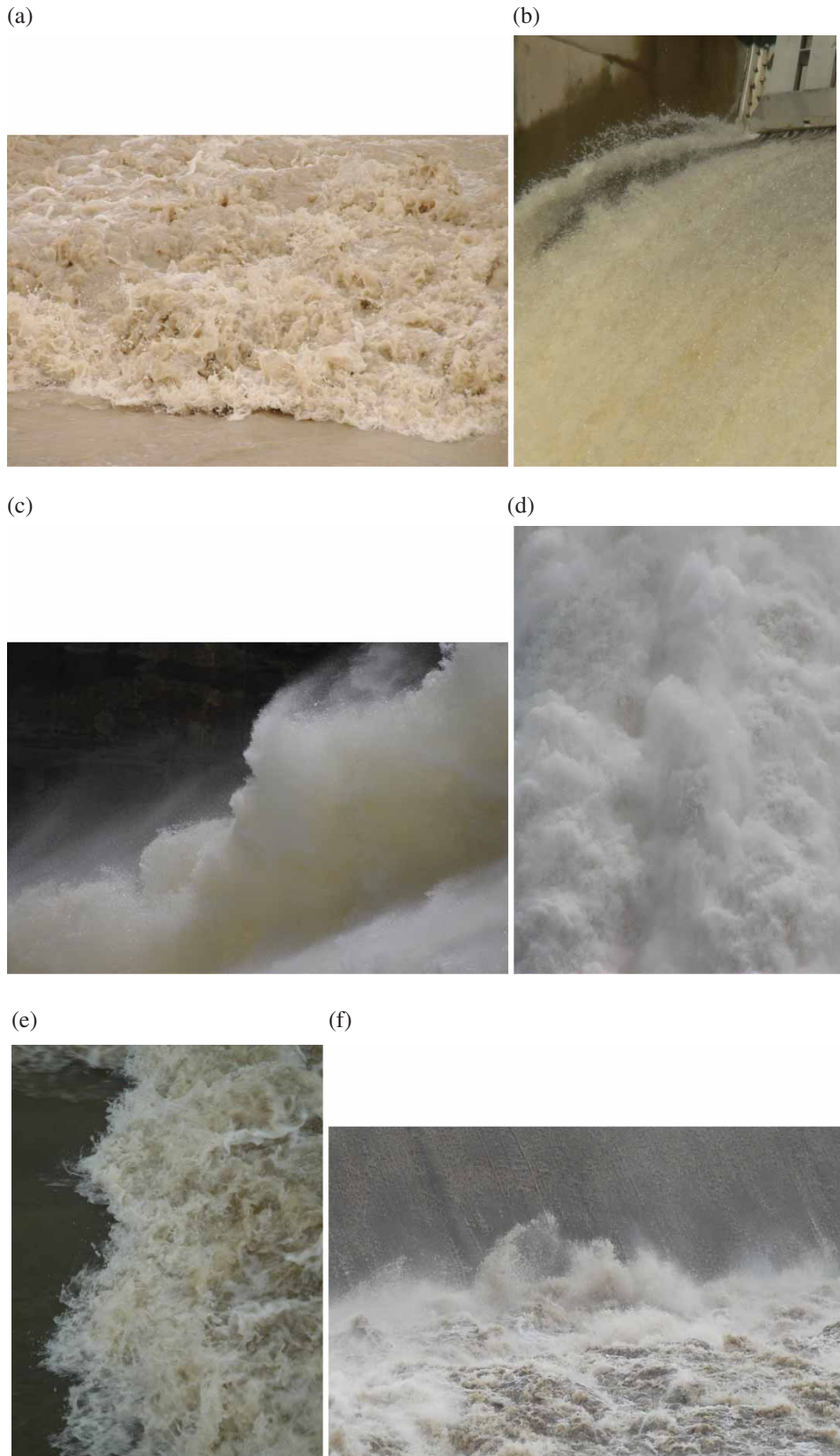


Figure 2 Small-scale flow features of aerated flows in hydraulic engineering: (a) hydraulic jump along Blake Snake Creek at Marburg (Australia) looking downstream on 11 January 2011, (b) the North Pine dam spillway flow (Australia) on 22 May 2009, (c) upper jet free-surface downstream of the Wivenhoe dam spillway flip bucket on 18 October 2010 (Australia) (shutter speed: 1/8,000 s), (d) upper free-surface of bottom outlet flow at the Three Gorges project (China) on 20 October 2004 ( $V = 35$  m/s, flow direction from bottom to top), (e) hydraulic jump roller in the Norman Creek culvert at the Ridge Street (Australia) on 20 May 2009 (flow direction from left to right) and (f) hydraulic jump at the toe of the Paradise Dam spillway (Australia) looking upstream on 30 December 2010 (Courtesy of André Chanson)

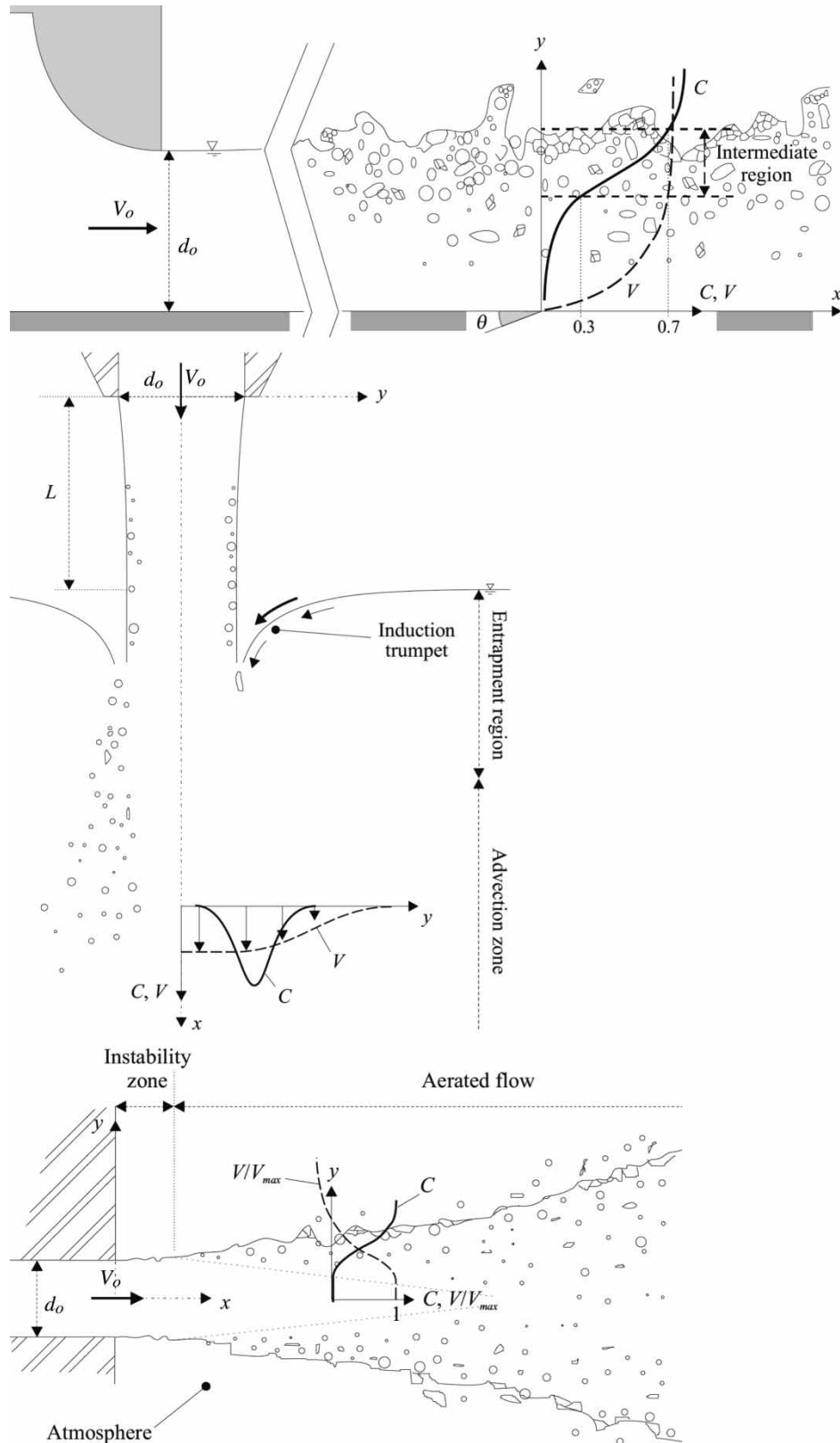


Figure 3 Sketch of a high-velocity free-surface flow. Top: interfacial aeration downstream of a bottom outlet; Middle: singular aeration at a vertical plunging jet; Bottom: interfacial aeration at a water jet discharging into the atmosphere

The entrainment of air may be either localized at some flow discontinuity or continuous along the free-surface: i.e. defined, respectively, as singular or interfacial aeration (Chanson 1997a). Figure 3 illustrates some seminal interfacial and singular aeration

processes, i.e. a self-aerated chute flow downstream of a gate outlet, a vertical plunging jet and a water jet discharging into atmosphere (from top to bottom). Figure 1b shows an example of interfacial aeration above the Wivenhoe dam spillway.

Examples of singular aeration are shown in hydraulic jumps at spillway toe and in rivers in flood (Figs 1d, 2a, 2e and 2f). In some applications, the free-surface aeration is maximized (e.g. for re-oxygenation in aeration cascades, drag reduction in naval applications). In other cases, aeration must be minimized or prevented: e.g. industrial jet cutting, fire-fighting. In most hydraulic engineering applications, the aeration is un-controlled (Figs 1 and 2), but the amount of entrained air and its mixing within the flow must be accurately predicted to optimize the system performance and to ensure a safe operation: “For many hydraulic structures, safe operation can only be achieved if not only the characteristics of the water flow are considered, but due attention is also given to the simultaneous movement of air in the system” (Wood 1991).

Over the last two decades, an increasing number of scientific contributions were published on aerated flow hydraulics. They reflect (a) a broader range of experimental configurations at laboratory scales, (b) availability of advanced off-the-shelf-instrumentation and (c) advancements in signal processing. The development of commercial instrumentation, with manufacturers in America, Asia and Europe, reflects the increased demand from the chemical and nuclear industries, enhancing capabilities of hydraulic laboratories. This trend has been complemented by some developments in basic signal processing (Chanson 2002, Chang *et al.* 2003, Chanson and Carosi 2007a). These advances provide a greater range of measured parameters (see below), thus improving capabilities for novel experiments and validation of numerical models.

## 2 Theoretical framework of aerated flows

When there is a sharp interface between immiscible fluids, i.e. air and water herein, the equations governing the multiphase gas–liquid flows at the micro-scale may be derived for each phase, and combined with some interface tracking (Tryggvason *et al.* 2011). Within a minimum set of restrictions, the equations of fluid motion in a conservative form are

$$\frac{\partial \rho_w}{\partial t} + \sum_{i=x,y,z} \frac{\partial(\rho_w v_{wi})}{\partial x_i} = 0 \quad \text{Water (1a)}$$

$$\frac{\partial \rho_a}{\partial t} + \sum_{i=x,y,z} \frac{\partial(\rho_a v_{ai})}{\partial x_i} = 0 \quad \text{Air (1b)}$$

$$\begin{aligned} \frac{\partial(\rho_w v_{wi})}{\partial t} + \sum_{j=x,y,z} \frac{\partial(\rho_w v_{wi} v_{wj})}{\partial x_j} &= -\frac{\partial p_w}{\partial x_i} + \rho_w g_i \\ &+ \sum_{j=x,y,z} \frac{\partial \tau_{wij}}{\partial x_j} \end{aligned} \quad \text{Water (2a)}$$

$$\begin{aligned} \frac{\partial(\rho_a v_{ai})}{\partial t} + \sum_{j=x,y,z} \frac{\partial(\rho_a v_{ai} v_{aj})}{\partial x_j} &= -\frac{\partial p_a}{\partial x_i} + \rho_a g_i \\ &+ \sum_{j=x,y,z} \frac{\partial \tau_{aj}}{\partial x_j} \end{aligned} \quad \text{Air (2b)}$$

where the subscripts *a* and *w* refer to the air and water properties, respectively, *v* is the instantaneous velocity component, *p* is the instantaneous pressure, *g<sub>i</sub>* is the gravity acceleration in the direction *i* = *x*, *y*, *z*, and *τ<sub>ij</sub>* denotes an instantaneous stress tensor. Equations (1a) and (2a) for water and Eqs. (1b) and (2b) for the air phase must be complemented by a mathematical representation of the moving interface and the associated conditions to couple the equations across the air–water interfaces. This formulation may be used for very detailed direct numerical simulations (DNS), although the application is very complicated (Tryggvason *et al.* 2011).

An alternative approach is based upon ensemble-averaged forms (3) and (4) of the conservation equations (1) and (2) for water and air (Drew and Passman 1999):

$$\frac{\partial((1 - C)\rho_w)}{\partial t} + \sum_{i=x,y,z} \frac{\partial((1 - C)\rho_w V_{wi})}{\partial x_i} = 0 \quad \text{Water (3a)}$$

$$\frac{\partial(C\rho_a)}{\partial t} + \sum_{i=x,y,z} \frac{\partial(C\rho_a V_{ai})}{\partial x_i} = 0 \quad \text{Air (3b)}$$

$$\begin{aligned} \frac{\partial((1 - C)\rho_w V_{wi})}{\partial t} + \sum_{j=x,y,z} \frac{\partial((1 - C)\rho_w V_{wi} V_{wj})}{\partial x_j} \\ = -(1 - C)\frac{\partial P}{\partial x_i} + (1 - C)\rho_w g_i \\ + \sum_{j=x,y,z} \frac{\partial((1 - C)(T_{wij} + T_{wij}^{EA}))}{\partial x_j} + M_{wi} \end{aligned} \quad \text{Water (4a)}$$

$$\begin{aligned} \frac{\partial(C\rho_a V_{ai})}{\partial t} + \sum_{j=x,y,z} \frac{\partial(C\rho_a V_{ai} V_{aj})}{\partial x_j} \\ = -C\frac{\partial P}{\partial x_i} + C\rho_a g_i + \sum_{j=x,y,z} \frac{\partial(C(T_{aj} + T_{aj}^{EA}))}{\partial x_j} + M_{ai} \end{aligned} \quad \text{Air (4b)}$$

where *C* is the averaged void fraction with the instantaneous void fraction *c* being 0 (water) or 1 (air), *V* and *P* are the mean velocity and pressure, respectively, *T<sub>ij</sub><sup>EA</sup>* is a stress tensor deriving from the averaging procedure and *M<sub>i</sub>* is the resultant force of the interactions of the phases (Bombardelli 2012). Any mass transfer between the two phases was ignored in Eqs. (3) and (4). Equation (4) is called the two-phase Navier–Stokes (N–S) equations or two fluid model (TFM).

Although the averaging of the conservation equations for each phase appears to give simpler expressions, a comparison between Eqs. (2) and (4) shows that the ensemble-averaging process adds two new terms in the right-hand side of Eq. (4). It is necessary, therefore, to derive a number of closure relationships, also called constitutive relationships, which imposes some significant consequences on the mathematical structure of the problem and represents an active research area (Drew and Passman 1999, Bombardelli 2012).

### 3 Modelling of aerated flows

The analytical and numerical studies of aerated flows in hydraulic engineering are difficult considering the large number of relevant equations, parameters and their complexity. Numerical simulations, which are typically based upon the two-phase N–S equations (i.e. TFM), are very demanding in terms of CPU time and computing facilities. Any solution of the (full) N–S equations in a free-surface air–water flow configuration is a real challenge because of the strong interface deformations and air entrainment (Lubin and Caltagirone 2009, Prosperetti and Tryggvason 2009). A recent research workshop concluded: “For most engineering applications, solving these equations will be impractical for the foreseeable future” (Hanratty *et al.* 2003). Current knowledge into aerated flows heavily relies upon laboratory investigations under controlled flow conditions (Wood 1991, Chanson 1997a). This is particularly important for on-going developments of numerical models and their validation (Lubin *et al.* 2009, Sousa *et al.* 2009, Ma *et al.* 2010, Bombardelli *et al.* 2011).

The validation of a numerical model must be based upon some data sets independent of those used for calibration. A number of studies discussed the intricacy of the validation process (Mehta 1998, Roache 1998, Rizzi and Vos 1998). In a complex situation, typical of aerated flows, the model outputs must be compared with a range of detailed gas–liquid flow properties including the distributions of void fraction, velocity, turbulence intensity and bubble sizes (Chanson and Lubin 2010). “*Unequivocally [ . . . ] experimental data are the sine qua non of validation; no experimental data means no validation*” (Roache 2009). The validation process must be physically sound as recommended by the American Institute of Aeronautics and Astronautics (AIAA 1998, Rizzi and Vos 1998, Roache 1998). Too many numerical studies lack credibility because they did not represent accurately the flow physics (Mehta 1998, Chanson and Lubin 2010). A key challenge is the uncertainty present in all physical systems. For example, in aerated flows, the data might be affected by the intrusive nature of the probes. More generally, the experimental data are subject to some intrinsic uncertainty, caused by a combination of technological limitations and accuracy of post-processing tools. The same applies to the numerical data, subjected to modelling, and numerical and round-off errors (Sagaut *et al.* 2008). An uncertainty analysis must be carried out for both physical and numerical data, and the quality of the validation process is closely linked to both. Many computational fluid dynamics (CFD) analyses to date fail to address the problem. Possibly because only a few mathematical techniques are presently mastered by the scientific community to analyse the results of the sensitivity analysis and to enhance the numerical solution accordingly (Roache 1998, 2009, Chanson and Lubin 2010).

Experimental investigations of air–water flows are not trivial (Rao and Kobus 1971), but some advances in metrology (e.g. phase-detection needle probes) combined with advanced post-processing techniques enable a detailed characterization of high-velocity aerated flows under controlled conditions (Cain and

Wood 1981a,b, Wood 1983,1985). A fundamental issue is the extrapolation of laboratory data to full-scale applications, associated with the selection of dynamic similarity, the usage of self-similarity and the development of theoretical relationships. The implications are broad because of the reliance of analytical and numerical modelling upon physical modelling for validation, especially in the absence of prototype data.

#### 3.1 Dimensional analysis and physical modelling of aerated flows

Any fundamental analysis of aerated flows in hydraulic engineering is based upon a large number of relevant equations to describe the two-phase turbulent flow motion. Physical modelling may provide some insights into the flow motion if a suitable dynamic similarity is selected (Novak and Cabelka 1981, Liggett 1994). For some singular aeration, the relevant dimensional parameters include the air and water physical properties and constants, the channel characteristics, the inflow conditions and the local two-phase flow properties at a location  $(x, y, z)$  (Kobus 1984, Wood 1991, Chanson 1997a, 2009). Considering a vertical circular plunging jet with inflow thickness  $d_o$  and velocity  $V_o$  (Fig. 3, middle), a simplified dimensional analysis yields, as a first approximation:

$$C, \frac{Fd_o}{V_o}, \frac{V}{\sqrt{gd_o}}, \frac{v'}{V_o}, \frac{d_{ab}}{d_o}, \frac{N_c d_o}{V_o}, \frac{T_{int}}{\sqrt{d_o/g}}, \frac{L_{int}}{d_o} \dots = F_1 \left( \frac{x}{d_o}, \frac{y}{d_o}, \frac{z}{d_o}, \frac{V_o}{\sqrt{gd_o}}, \rho_w \frac{V_o d_o}{\mu_w}, \frac{g \mu_w^2}{\rho_w \sigma^4}, \frac{L}{d_o}, \frac{v'_o}{V_o}, \dots \right) \quad (5)$$

where  $C$  is the void fraction,  $V$  is the interfacial velocity,  $v'$  is a characteristic turbulent velocity,  $F$  is the bubble count rate defined as the number of bubbles detected per second in a small control volume,  $d_{ab}$  is a characteristic bubble size,  $N_c$  is the number of bubble clusters per second,  $T_{int}$  and  $L_{int}$  are some turbulent integral time and length scales, respectively,  $x$  is the longitudinal coordinate,  $y$  is the radial coordinate and  $z$  is the ortho-radial coordinate both measured from the jet centreline,  $\mu_w$  is the water dynamic viscosity,  $\sigma$  is the surface tension between air and water,  $d_o$  is the jet diameter,  $V_o$  is the nozzle velocity,  $L$  is the free-jet length and  $v'_o$  is a characteristic turbulent velocity at the inflow.

For an interfacial flow such as gated spillway flow in a rectangular chute (Fig. 3, top), a simplified dimensional analysis gives

$$C, \frac{Fd_c}{V_c}, \frac{V}{\sqrt{gd_c}}, \frac{v'}{V_c}, \frac{d_{ab}}{d_c}, \frac{N_c d_c}{V_c}, \frac{T_{int}}{\sqrt{d_c/g}}, \frac{L_{int}}{d_c} \dots = F_2 \left( \frac{x}{d_c}, \frac{y}{d_c}, \frac{z}{d_c}, \frac{d_c}{k_s}, \rho_w \frac{\sqrt{gd_c^3}}{\mu_w}, \frac{g \mu_w^4}{\rho_w \sigma^3}, \frac{d_o}{d_c}, \frac{V_o}{V_c}, \frac{v'_o}{V_c}, \frac{W}{d_c}, \theta, \dots \right) \quad (6)$$

where  $k_s$  is an equivalent roughness height,  $d_o$  is the gate opening,  $V_o$  is the gate velocity,  $W$  is the chute width,  $\theta$  is the chute slope

and  $d_c$  is the critical flow depth defined as

$$d_c = \sqrt[3]{\frac{Q_w^2}{g W^2}} \quad (7)$$

and  $V_c$  is the critical flow velocity:

$$V_c = \sqrt[3]{\frac{g Q_w}{W}} \quad (8)$$

In Eq. (6), the critical flow depth and velocity,  $d_c$  and  $V_c$ , respectively, were selected as the relevant length and velocity scales, thus assuming implicitly a Froude similitude since the dimensionless ratio  $d_c/k_s$  is proportional to a roughness Froude number.

Equations (5) and (6) express the turbulent-aerated flow properties at a position  $(x, y, z)$  within the gas–liquid flow as functions of a number of dimensionless parameters, including the Froude number  $F$  (fourth term in right-hand-side term of Eq. 5), the Reynolds number  $R$  (fifth term) and the Morton number  $Mo$  (sixth term), which is a combination of the Froude  $F$ , Reynolds  $R$  and Weber  $We$  numbers:

$$Mo = \frac{g \mu_w^2}{\rho_w \sigma^4} = \frac{We^3}{F^2 R^4} \quad (9)$$

Since the  $\Pi$ -Buckingham theorem states that any dimensionless number can be replaced by a combination of itself and other dimensionless numbers, Eqs. (5) and (6) are expressed in terms of the Morton number and thus the Weber number is not considered. The Morton number is a constant in most hydraulic modelling studies because both laboratory and full-scale prototype flows use the same fluids, i.e. air and water. Note that the effects of surfactants and bio-chemicals on the air entrainment process and two-phase flow properties were neglected in the above developments. Reif (1978) and Chanson *et al.* (2006) tested, respectively, the effects of surfactants in hydraulic jumps and bio-chemicals in vertical circular plunging jets. Their results demonstrated some substantial modulation of the air–water flow properties which were implicitly ignored in Eqs. (5) and (6). Further, the effects of intrusive probes onto the flow were neglected. For phase-detection needle probes, this was recently considered (Chanson and Toombes 2002, Gonzalez 2005, Carosi and Chanson 2006) and the results indicate some non-negligible impact of the sensor size on the detection of small bubbles, especially sub-millimetre ones.

Traditionally, the free-surface flows including plunging jets and self-aerated chute flows are studied based on a Froude similarity (Henderson 1966, Liggett 1994, Chanson 2004b, Viollet *et al.* 2002). In the particular case of a hydraulic jump, basic momentum considerations demonstrate the significance of the inflow Froude number (Bélanger 1841, Lighthill 1978) and the selection of the Froude similitude follows implicitly from basic theoretical considerations (Liggett 1994, Chanson 2012). However, the turbulent shear flows are dominated by viscous effects,

while the mechanisms of bubble breakup and coalescence are dominated by surface tension forces. Thus, a true dynamic similarity of aerated flow does require achieving identical Froude, Reynolds and Morton numbers in both the prototype and its model. This is impossible to achieve using geometrically similar models unless working at the full-scale. Practically, the Froude and Morton dynamic similarities are simultaneously employed when the same fluids (air and water) are used in the prototype and model. But the Reynolds number is grossly low in laboratory conditions, thus leading to viscous-scale effects in small-size models typical of hydraulic engineering applications (Kobus 1984, Wood 1991, Chanson 2009). Figure 4 illustrates two examples: a water jet discharging into atmosphere (Fig. 4a) and a dropshaft flow (Fig. 4b). In each case, a drastic reduction in flow aeration is observed in the smaller model operating at smaller Reynolds numbers for the identical Froude and Morton numbers.

Only a few studies systematically investigated the aerated flow properties, at the local sub-millimetre scale, in geometrically similar models under controlled flow conditions to assess the associated-scale effects. These studies were based upon the Froude and Morton similitudes with undistorted models, encompassing vertical plunging jets (Chanson *et al.* 2004), hydraulic jumps (Chanson and Gualtieri 2008, Murzyn and Chanson 2008, Chanson and Chachereau 2013), dropshafts (Chanson 2004d), spillway aeration devices (Pfister and Hager 2010) and stepped spillways (Boes and Hager 2003, Chanson and Gonzalez 2005, Felder and Chanson 2009). Despite the limited scope, the results of experimental investigations demonstrated unequivocally the limitations of dynamic similarity and physical modelling of aerated flows. They emphasized further that the selection of the criteria to assess scale affects is critical and should involve a range of characteristics such as void fraction distributions, turbulence intensity distributions and distributions of bubble chords (Chanson 2009, Chanson and Chachereau 2013). The experimental results show that some parameters, such as bubble sizes and turbulent scales, are likely to be affected by scale effects, even in 2:1 to 3:1 scale models (Chanson 2004b, 2009). No scale effect is observed at full-scale only, using the same fluids in prototype and model, i.e. in prototype flow conditions.

### 3.2 Self-similarity in aerated flows

If spatial distributions of flow properties at various times (or/and spatial locations) can be obtained from one another by a similarity transformation, then it is said that a process possesses a self-similarity property (Barenblatt 1996). Self-similarity is a powerful concept in the turbulent flow research involving a wide spectrum of spatial and temporal scales, and hydraulic engineering applications encompass turbulent flows with a broad range of length and time scales. The non-linear interactions between turbulent vortices and particles at different scales lead to a complicated flow structure, and relationships among flow properties at different scales are of crucial importance (Wang



Figure 4 Scale effects in aerated flow situations. Flow direction from left to right on all photographs. (a) Water jet discharging into the atmosphere. Left: the Three Gorges Project,  $V_o = 35$  m/s,  $V_o/(gd_o)^{1/2} = 4.2$ ,  $\rho_w q_w/\mu_w = 2.8 \times 10^8$ ,  $g\mu_w^2/(\rho_w\sigma^4) = 3.4 \times 10^{-4}$ , shutter speed: 1/1,000 s. Right: Laboratory study:  $V_o = 4.1$  m/s,  $V_o/(gd_o)^{1/2} = 4.1$ ,  $\rho_w q_w/\mu_w = 4.3 \times 10^5$ ,  $g\mu_w^2/(\rho_w\sigma^4) = 3.4 \times 10^{-4}$ . (b) Vertical dropshaft. Left: full-scale,  $V_o = 1.1$  m/s,  $V_o/(gd_o)^{1/2} = 1$ ,  $\rho_w q_w/\mu_w = 1.4 \times 10^5$ ,  $g\mu_w^2/(\rho_w\sigma^4) = 3.4 \times 10^{-4}$ , shutter speed: 1/30 s. Right: 3.1:1 scale model:  $V_o = 0.57$  m/s,  $V_o/(gd_o)^{1/2} = 1$ ,  $\rho_w q_w/\mu_w = 1.8 \times 10^4$ ,  $g\mu_w^2/(\rho_w\sigma^4) = 3.4 \times 10^{-4}$ , shutter speed: 1/60 s

1998, Barenblatt 1996). These relationships play also a major role in comparing analytical, experimental and numerical results if these results relate to different scales. In some recent studies, self-similarity was tested systematically in terms of the distributions of air–water flow properties in skimming flows on stepped spillways (Chanson and Carosi 2007b, Felder and Chanson 2009). Several self-similar relationships were observed at both macroscopic and sub-millimetre scales.

Self-similarity is closely linked to dynamic and kinematic similarities, and the existence of self-similar relationships may have major implications on the measurement strategy in experimental and physical modelling studies (Foss *et al.* 2007). Although it is nearly impossible to achieve a true dynamic similarity in aerated flows because of the number of relevant dimensionless parameters (see the previous section), these experimental findings showed a number of self-similar relationships that remain invariant under changes of scale. Namely, they have

scaling symmetry which in turn led to remarkable applications at prototype scales. These results may provide a picture general enough to be used, as a first approximation, to characterize the aerated flow field in similar hydraulic structures irrespective of the physical scale (Felder and Chanson 2009).

### 3.3 Discussion

The modelling of aerated flows is presently restricted by the complexity of theoretical equations, some limitations of numerical techniques, a lack of full-scale prototype data and very-limited detailed experimental data sets suitable for sound CFD model validation. The implications are far reaching, especially for numerical simulations, i.e. can we trust numerical modelling whose validation is based upon small-size scale-affected laboratory data? The findings of systematic experimental studies demonstrated that (a) the notion of scale effects must be defined

in terms of some specific set of gas–liquid characteristics, and (b) some aerated flow properties are more affected by scale effects than others, even in large-size facilities. Interestingly, distorted physical modelling of aerated flows has not been considered to date, although the scale distortion may enable to achieve some similitude in terms of bubble rise velocity on chute spillways and inclined plunging jets.

There are some basic differences between dynamic similarity and self-similarity, and Fig. 5 provides some illustration. Figure 5a presents some dimensionless distributions of void fractions in chute spillways, with a selection of the dimensionless terms based upon an undistorted Froude similitude. The results show a close agreement between prototype and model data, although the model Reynolds numbers were an order of magnitude smaller than prototype Reynolds numbers (Fig. 5a). In this instance, the findings imply that the laboratory data may be extrapolated, based upon a Froude similitude, to a full-scale with the negligible scale effect. Figure 5b shows some self-similar relationship in terms of interfacial velocity distributions in self-aerated smooth chute flows. The results highlighted a sound self-similarity expressed in the form of a power law for  $y/Y_{90} < 1$  and a uniform profile above:

$$\frac{V}{V_{90}} = \left(\frac{y}{Y_{90}}\right)^{1/N} \quad y/Y_{90} < 1 \quad (10)$$

$$\frac{V}{V_{90}} = 1 \quad y/Y_{90} > 1 \quad (11)$$

where  $Y_{90}$  is the characteristic distance from invert where  $C = 0.90$ , and  $V_{90}$  is the characteristic velocity at  $y = Y_{90}$ . Despite a close agreement between the prototype and model data (Fig. 5b), the laboratory results should not be extrapolated to the full-scale, unless the scaling relationships in terms of the characteristic distance  $Y_{90}$  and velocity  $V_{90}$  are known. If one or the other cannot be extrapolated based upon similarity considerations, the self-similarity may not assist with the engineering design.

In addition to the dynamic similarity and self-similarity, a further modelling approach may be based upon some theoretical developments leading to theoretically-based equations. An illustration is shown in Fig. 5a, in which the void fraction distributions are compared with an analytical solution of the advection–diffusion equation for air bubbles (dashed line in Fig. 5). Following Rouse (1937) for suspended sediment flows and Wood (1985) for self-aerated chute flows, a number of theoretical void fraction distributions were derived analytically for self-aerated chute flows, water jets discharging into air, plunging jets and hydraulic jumps (Chanson 1997a, 2008). Recent developments included Chanson and Toombes (2002) for self-aerated skimming flows on stepped spillways, and Chanson (2010) for hydraulic jumps. The existence of theoretical relationships may have some implications for the laboratory studies

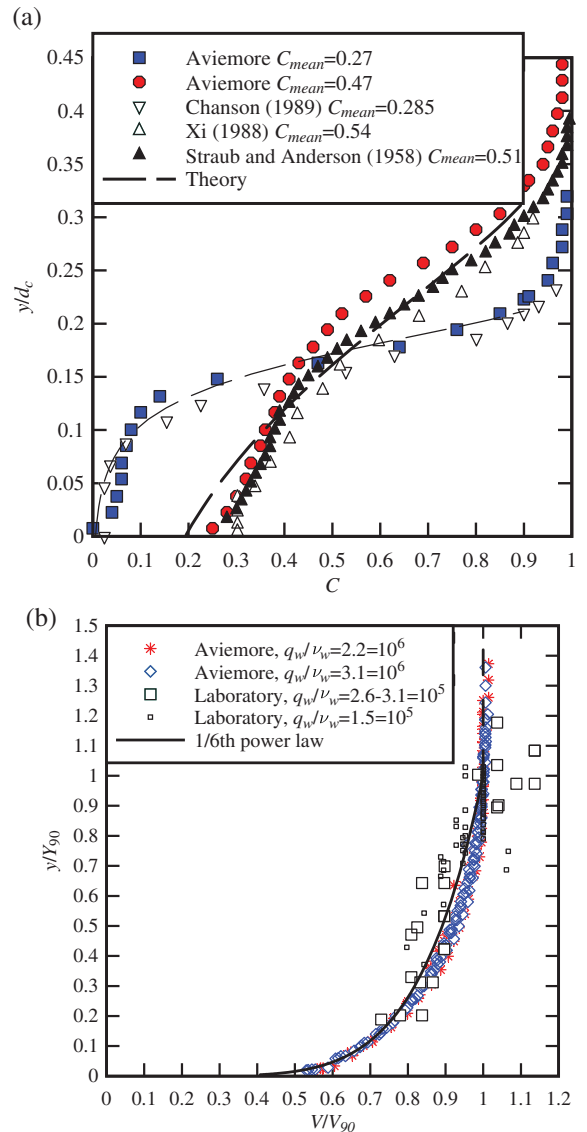


Figure 5 Froude similar and self-similar data presentation in self-aerated smooth chute flows. Prototype data: the Aviemore dam spillway (Cain 1978); Laboratory data: Straub and Anderson (1958), Xi (1988), Chanson (1989, 1997b). (a) Froude similar distributions of void fractions. Comparison with a theoretical model (Chanson 1997a). (b) Self-similar interfacial velocity distributions

Data set	$\theta$ (°)	$C_{mean}$	$V_{90}$ (m/s)	$\rho_w q_w / \mu_w$
Aviemore dam	45	0.27	18.2	$2.2 \times 10^6$
		0.47	20.2	$2.2 \times 10^6$
Chanson (1989)	52.3	0.285	11.3	$2.6 \times 10^5$
Xi (1988)	52.5	0.54	–	$3.2 \times 10^5$
Straub and Anderson (1958)	45	0.51	–	$6.9 \times 10^5$

and measurement methods. For example, for self-aerated chute flows (Fig. 5a), the analytical solution of the advection diffusion equation implies that the void fraction distribution is given by  $C = f(y/Y_{90}, C_{mean})$ , where  $C_{mean}$  is the depth-averaged void fraction; this analytical solution implies that no additional measurements are needed in regions of identical mean void fraction

$C_{mean}$  for an identical discharge per unit width. Thus, the analytical solutions may allow a drastic reduction of the volume of measurements.

#### 4 Metrology of air–water flows

##### 4.1 Instrumentation

In a free-surface flow, the void fraction ranges from 0 to 100%, and the mass and momentum fluxes are encompassed within the flow region with void fractions less than 95% (Cain 1978, Wood 1985). In this zone ( $C < 0.95$ ), a number of field and laboratory data sets demonstrated that the high-velocity gas–liquid flows behave as a quasi-homogenous mixture and the two phases travel with a nearly identical velocity, i.e. the slip velocity is negligible (Rao and Kobus 1971, Cain and Wood 1981b, Chanson 1997a). Any detailed characterization of the entire gas–liquid flow must rely on instrumentation, applicable and accurate for a wide range of the void fraction levels ( $0 < C < 0.95$ ).

In a two-phase air–water flow, a description of the turbulent flow field requires a number of parameters significantly larger than for a monophasic flow. The additional parameters include the void fraction, the bubble count rate, the bubble and drop size distributions, the clustering properties. Further, a number of parameters (e.g. instantaneous velocity) cannot be measured with typically available instruments (Pitot tube, acoustic Doppler velocimetry (ADV), laser Doppler velocimetry (LDA)) because the presence of bubbles and air–water interfaces affects adversely their operation. With void fractions less than 3% (or even less), some measurement techniques may be used, although with some empirical corrections: e.g. photography, Pitot tube, ADV, LDA (Sheng and Irons 1991, Liu *et al.* 2004). However, the corrections of such type of measurements are highly empirical and rely upon the intrinsic performances of the measurement devices. This “correction” approach should never be used for void fractions larger than 3 to 5%, and it is inappropriate for many free-surface flows in which the local void fractions range up to 100%. Recent developments in particle image velocimetry provided detailed data in dilute disperse flows (Balachandar and Eaton 2010), but for the limited flow conditions corresponding to void/liquid fractions less than about 5%.

Some specialized instrumentation was developed during the last 50 years, including back-flushing Pitot tubes, needle phase-detection probes, conical hot-film probes and fibre phase Doppler anemometry. The needle probe and conical hot-film systems are the two oldest techniques. The conical hot-film probes have been used for 40 years with a range of flow conditions, including hydraulic jumps (Resch and Leutheusser 1972, Babb and Aus 1981), vertical plunging jets (Chanson and Brattberg 1998) and bubble-induced turbulence (Lance and Bataille 1991, Rensen *et al.* 2005). A major constraint of the hot-film instrumentation is the calibration of the sensor, as well as the rapid probe contamination requiring systematic re-calibrations (e.g. every three minutes if Brisbane tap water is used) (Chanson and Brattberg

1998). The use of demineralized water may significantly reduce the probe sensor contamination rate, although this restricts drastically the test facility size, hence the Reynolds number. Some pertinent reviews of air–water flow probes and their operational issues include Jones and Delhay (1976), Cartellier and Achard (1991) and Chanson (2002).

Over the past 40 years, most successful (and most numerous) experiments have been conducted with phase-detection needle probes, including some milestone prototype measurements on the Aviemore dam spillway in New Zealand (Cain and Wood 1981a,b). The needle-shaped phase-detection probe is designed to pierce the bubbles and droplets (Fig. 6). It is particularly

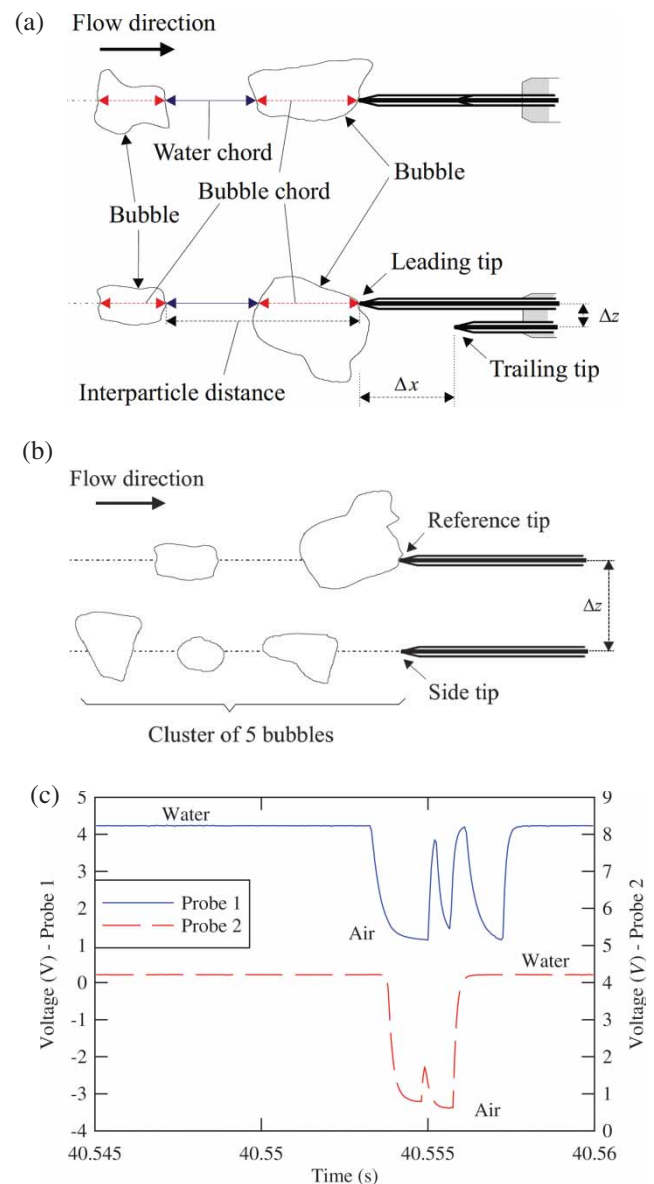


Figure 6 Phase-detection needle-type probes. (a) Double-tip probe (side view and view in elevation). (b) Cluster of five bubbles passing an array of two side-by-side single-tip probes (view in elevation). (c) Instantaneous voltage signal recorded by an array of two side-by-side needle probes. Data: Chanson and Carosi (2007b),  $d_c/h = 1.45$ ,  $\rho_w q_w t / \mu_w = 1.7 \times 10^5$ , step edge 10,  $y = 0.095$  m,  $C = 0.022$  and  $F = 35.6$  Hz (reference probe),  $V = 3.4$  m/s,  $\Delta z = 3.6$  mm

well-suited to track interfaces, to provide data for the validation of DNS. Since its introduction in experimental practice by Neal and Bankoff (1963, 1965), the designs of the needle probe have been refined. Although the first designs were based on resistivity sensors, both optical fibre and resistivity sensors are currently used (Cartellier 1992, Chanson 2002). In practice, the signal output quality of phase-detection intrusive probes is closely linked to the sensor size, the sampling rate  $F_{\text{sampl}}$  and sampling duration  $T_{\text{sampl}}$ . The size of the sensor is basically the needle diameter  $\varnothing_{\text{tip}}$ , which is the diameter of the optical fibre or inner electrode. Current measurement systems use sensor sizes less than 0.1 mm at low flow velocities ( $V < 1$  to 2 m/s), while the studies of high velocity flows ( $1 < V < 20$  m/s and higher) require more sturdy probes with diameters typically between 0.1 and 0.5 mm. As an example, the author used 0.025 mm needle probes at flow velocities up to 9 m/s, but the risks of probe damage were high with velocities larger than 3 m/s (Cummings and Chanson 1997b, Brattberg and Chanson 1998, Chanson and Brattberg 2000); he also used needle probes with inner electrodes between 0.1 and 0.35 mm in highly turbulent flows with velocities up to 18.5 m/s without any trouble (Chanson 1989, 2002). With a needle probe, the selection of the sampling frequency is linked to the smallest detectable bubble size, which is of the order of magnitude of the needle diameter  $\varnothing_{\text{tip}}$ . This yields a minimum sampling frequency to prevent aliasing:

$$F_{\text{sampl}} > 2 \frac{V}{\varnothing_{\text{tip}}} \quad (12)$$

where  $V$  is the longitudinal velocity. Some in-depth sensitivity analyses were conducted in terms of the sampling frequency and duration in hydraulic jumps and stepped chutes (Chanson 2007c, Chanson and Felder 2010). The results showed that the sampling rate had to be greater than 10 kHz, and the sampling duration greater than 20 s to have negligible effects on the void fraction, bubble count rate and air–water velocity measurements, while more advanced correlation analyses including the estimate of the turbulence intensity require a sampling duration of 45 s or larger. A dual-tip probe provides additional information on the interfacial velocity and turbulence level. With such a dual-tip probe, two key probe characteristics are the longitudinal  $\Delta x$  and transverse  $\Delta z$  separation distances of the sensors. Figure 6a shows a dual-tip probe designed at the University of Queensland to minimize the effect of the leading tip onto the bubble piercing by the trailing tip. The wake effects of the leading tip on the trailing tip were discussed by Sene (1984) and Chanson (1988). Cummings (1996) tested the effects of the transverse separation distance on the data outputs, and he obtained optimum results with  $\Delta z/\Delta x = 0.08 - 0.10$ . Some measurement experience is summarised in Fig. 7 in terms of the longitudinal distance between probes and sensor size. The data tend to imply that an optimum longitudinal separation distance is linked to the interfacial velocity and

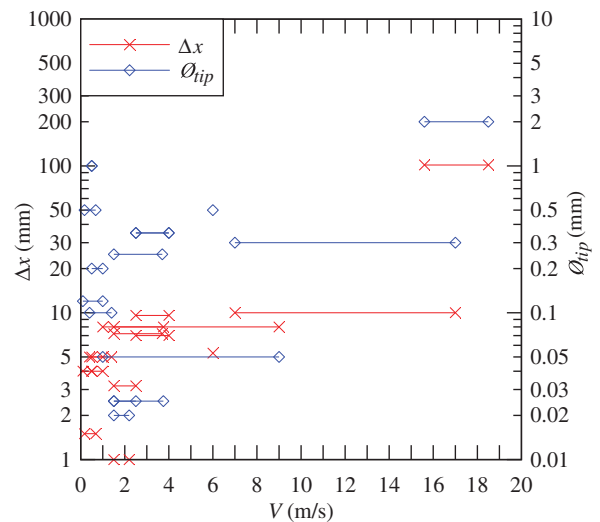


Figure 7 Longitudinal separation distance  $\Delta x$  and probe sensor size  $\varnothing_{\text{tip}}$  of dual tip needle probes. Experimental experiences in prototype (Cain and Wood 1981a) and laboratory

sensor size:

$$\frac{(\Delta x)_{\text{optimum}}}{\varnothing_{\text{tip}}} \approx 33.5 V^{0.27} \quad (13)$$

This result was obtained for  $0.4 < V < 18.5$  m/s and  $1.5 < \Delta x < 102$  mm. The experience indicates that the longitudinal separation distance  $\Delta x$  impacted only mildly on the data quality, as hinted in Fig. 7.

While the single-tip and dual-tip needle probe designs are most common, other probe designs were also successfully tested. These include three or four sensor needle probes (Kim *et al.* 2000), a cylindrical probe for cross flow turbine measurements (Borges *et al.* 2010), single-tip probe arrays (Coakley *et al.* 2001, Chanson 2004c, 2007b), and other electrical probes (Lamb and Killen 1950, Straub and Lamb 1956).

#### 4.2 Signal processing

Figure 6c illustrates a typical signal output from an array of two single-tip needle probes similar to the one shown in Fig. 6b. In Fig. 6c, each steep drop of the signal corresponds to an air bubble interface pierced by the probe tip and the graph shows a group of five bubbles detected by the probes. Although the probe response to bubble piercing should be ideally rectangular, the signal output is not exactly that because of the finite size of the tip, the wetting/drying time of the interface covering the tip and the response time of the probe and electronics. The measured raw signal is typically transformed into a binary time-series of instantaneous void fraction ( $c = 0$  in water and 1 in air). Although there are several phase discrimination techniques, the most robust technique for free-surface flows is the single-threshold technique, with a threshold set at 40 to 60% of the air–water range (Toombes 2002, Chanson and Felder 2010, Felder 2013).

In a steady stationary flow, the time-averaged void fraction  $C$  is the arithmetic mean of the instantaneous void fraction. The bubble count rate  $F$  is the number of bubbles (i.e. water-to-air interfaces) detected by the probe sensor per second. With a dual-tip probe (Fig. 6a), the time-averaged velocity is deduced from the cross-correlation function between the probe signals:

$$V = \frac{\Delta x}{T} \tag{14}$$

where  $T$  is the average interfacial travel time between the sensors corresponding to the time lag of the maximum cross-correlation function  $(R_{xy})_{max}$  (Fig. 8). The shape of the auto- and cross-correlation functions provides further information on the turbulent field, including the auto- and cross-correlation integral time scales  $T_{xx}$  and  $T_{xy}$  (Fig. 8), and the turbulence intensity (Chanson and Carosi 2007a, Felder and Chanson 2012):

$$Tu = \frac{v'}{V} = \frac{\sqrt{2}}{\sqrt{\pi}T} \sqrt{\left(\frac{T_{xy}}{(R_{xy})_{max}}\right)^2 - T_{xx}^2} \tag{15}$$

Assuming that the cross-correlation function is a Gaussian distribution and defining  $\tau_{0.5}$  as the time scale for which  $R_{oxy}(T + \tau_{0.5}) = R_{xy}(T)/2$  and  $T_{0.5}$  is the characteristic time for which the normalized autocorrelation function equals 0.5 (Fig. 8), Eq. (15) may be simplified into (Chanson and Toombes 2002):

$$\frac{v'}{V} = 0.851 \frac{\sqrt{\tau_{0.5}^2 - T_{0.5}^2}}{T} \tag{16}$$

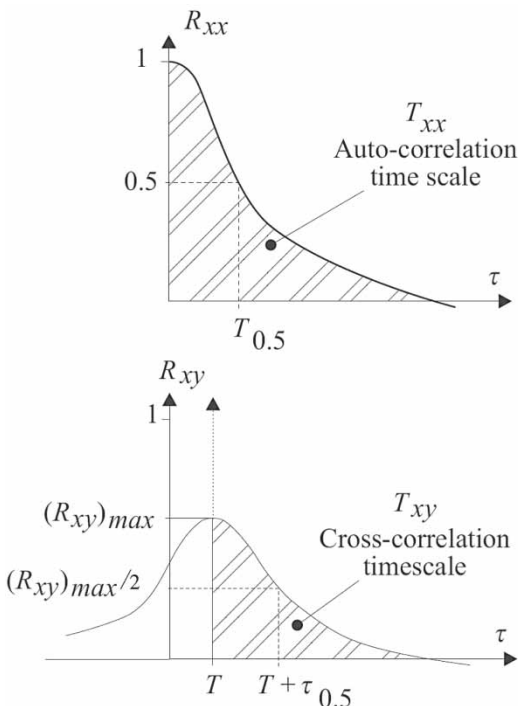


Figure 8 Definition sketch of auto- and cross-correlation functions

Equations (15) and (16) are based upon the assumption that both auto- and cross-correlation functions have a Gaussian shape, and laboratory observations showed that the approximation is reasonable for small-to-moderate time lags  $\tau$ . When an array of two sensors are mounted side by side separated by a transverse distance  $\Delta z$  (Fig. 6b) and the measurements are performed for a range of separation distances, the (transverse) integral length and time scales,  $L_{int}$  and  $T_{int}$ , respectively, may be calculated as

$$L_{int} = \int_{z=0}^{z((R_{xz})_{max}=0)} (R_{xz})_{max} dz \tag{17}$$

$$T_{int} = \frac{1}{L_{int}} \int_{z=0}^{z((R_{xz})_{max}=0)} (R_{xz})_{max} T_{xz} dz \tag{18}$$

where  $(R_{xz})_{max}$  and  $T_{xz}$  are the maximum cross-correlation coefficient and cross-correlation integral time scale (Chanson 2007b, Chanson and Carosi 2007b). Parameters  $L_{int}$  and  $T_{int}$  are characteristics of the large vortical structures advecting the air bubbles and interacting with the air–water interfaces. Detailed experimental data were obtained in hydraulic jumps (Chanson 2007b, Zhang *et al.* 2013) and stepped chute flows (Chanson and Carosi 2007b, Felder and Chanson 2009). The results highlighted the importance of the intermediate air–water flow region, where  $0.3 < C < 0.7$ , in which the turbulence intensity, turbulent integral time and length scales were maximum. This is illustrated in Fig. 9 for a skimming flow on a stepped spillway:  $Tu$ ,  $T_{int}$  and  $L_{int}$  are shown as functions of the time-averaged void fraction  $C$ . The above method may also be applied in the longitudinal direction by varying the separation distance  $\Delta x$ . Experiments in skimming flow above a stepped chute yielded close results in terms of turbulent integral scales between the longitudinal and transverse separation distances (Chanson and Carosi 2007b).

The signal processing of needle probe outcomes may also provide information on the microscopic structure of the gas–liquid flow. Microscopic properties include the distributions of air and water chords at each sampling location, as well as the sequential arrangement of air and water chords (Fig. 6). The latter may allow the characterization of bubble and droplet clustering, including the cluster properties. The study of particle clustering is relevant in industrial applications to infer whether the formation frequency responds to some particular frequencies of the flow. The level of clustering may give a measure of the magnitude of bubble–turbulence interactions and associated turbulent dissipation. In the bubbly flow region ( $C < 0.3$ ), clustering is linked with both turbulent particle clustering and the effects of inertial forces leading to bubble trapping and clustering in large-scale turbulent structures. It may result from the self-excitation of fluctuations of the bubble concentration (Elperin *et al.* 1996) and particle–particle interactions (i.e. near-wake effect). When a bubble is trapped in a vortical structure, the centrifugal pressure gradient moves the bubble inside the coherent structure core where bubble–bubble interactions may further take place

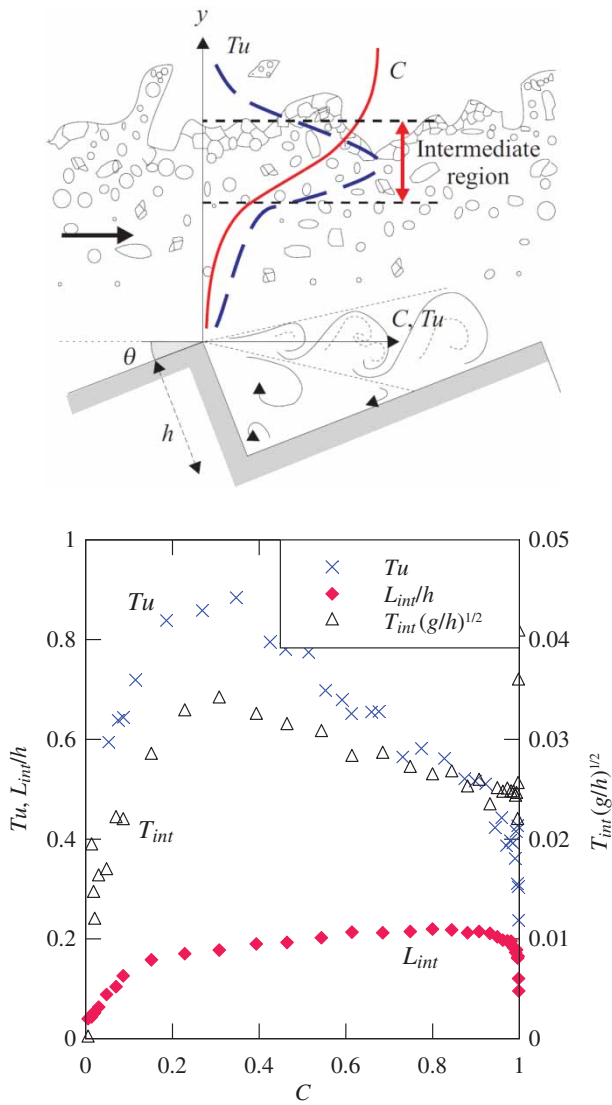


Figure 9 Air-water skimming flow on a stepped spillway in the intermediate region ( $0.3 < C < 0.7$ ). Data: Felder and Chanson (2009),  $\theta = 21.8^\circ$ ,  $h = 0.05$  m,  $d_c/h = 2.39$ ,  $\rho_w q_w / \mu_w = 1.3 \times 10^5$ , step edge 18

(Tooby *et al.* 1977, Sene *et al.* 1994). Note that particle clustering analyses are typically restricted to the bubbly and spray region,  $C < 0.3$  and  $C > 0.7$ , respectively.

There are two main types of signal analyses to investigate particle clustering. One method is based upon the analysis of the water chord between two adjacent air bubbles. If two particles are closer than a characteristic length scale, they may form a bubble cluster. This characteristic length scale may be related to the water chord statistics or to the lead bubble size itself, since bubbles within that distance are in the near-wake of and influenced by the leading bubble. A number of early studies were conducted in hydraulic jumps, dropshaft flows and stepped spillway flows (Chanson and Toombes 2002, Chanson *et al.* 2006, Gualtieri and Chanson 2007, 2010). These studies were restricted to the streamwise distribution of bubbles and did not take into account particles travelling side by side or a group of spatially distributed particles (Fig. 6b). A recent numerical

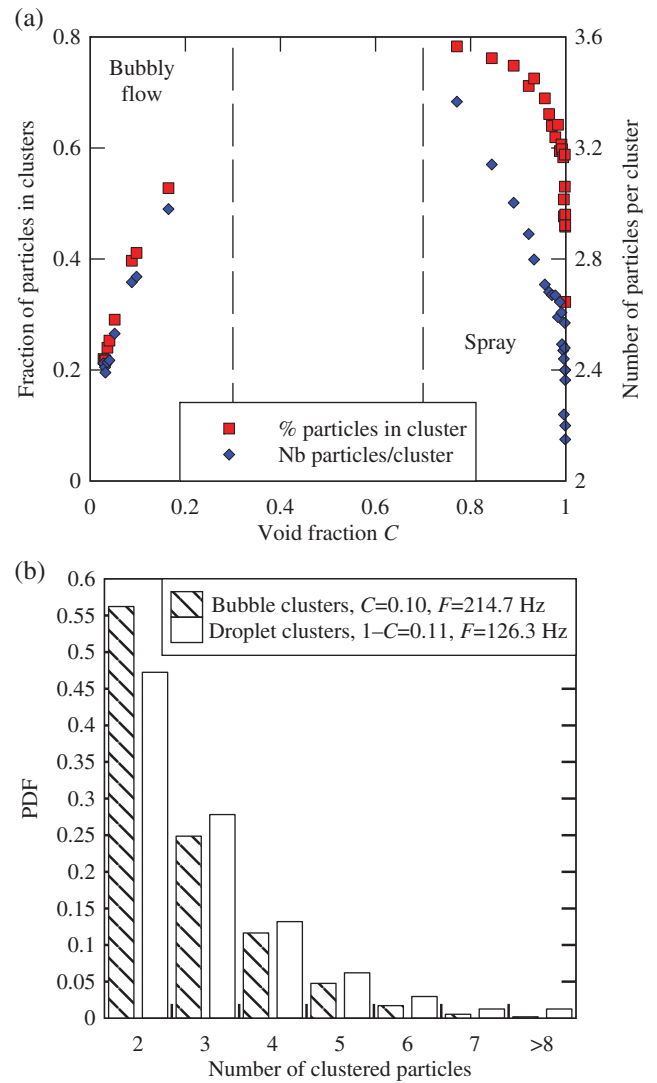


Figure 10 Clustering characteristics in a skimming flow above a stepped chute: bubble clusters in bubbly region ( $C < 0.3$ ) and droplet clusters counted in spray region ( $C > 0.7$ ). Data: Sun and Chanson (2013), Chanson and Carosi (2007b),  $\theta = 21.8^\circ$ ,  $h = 0.10$  m,  $d_c/h = 1.15$ ,  $\rho_w q_w / \mu_w = 1.2 \times 10^5$ , step edge 10, transverse probe spacing  $\Delta z = 3.6$  mm. (a) Fraction of particles in clusters (left axis) and average number of particle per cluster (right axis) as functions of void fraction. (b) Probability distribution functions of number of bubbles/droplets per cluster for a comparable void/liquid fraction

study using an Eulerian–Lagrangian approach showed that the longitudinal signal analysis may be representative of the three-dimensional flow (Calzavarini *et al.* 2008). An experimental study of bubbles/droplets using two probes located side by side in skimming flow above a stepped spillway yielded comparable results, although the data highlighted some complex interaction between entrained air and turbulent structures (Sun and Chanson 2013). Figure 10a presents some cluster properties in a skimming flow on a stepped spillway, and Fig. 10b shows the distribution of number of particles per cluster.

Another method is based upon an analysis of interparticle distance (Fig. 6a). In an ideal randomly dispersed flow, the distribution of interparticle distances (and arrival times)

follows a Poisson distribution, assuming non-interacting point particles (Edwards and Marx 1995a, Noymer 2000, Heinlein and Fritsching 2006). Any deviation from a Poisson process indicates some non-random dispersed structure, hence particle clustering, and the degree of non-random particle clustering may be quantified by Chi-square tests. For an ideal dispersed flow driven by a superposition of Poisson-distributed bubble sizes, the interparticle time distribution function is

$$f(t) = \frac{F^2(T_{\text{sampl}} - t) \exp(-Ft)}{FT_{\text{sampl}} - 1 + \exp(-F T_{\text{sampl}})} \quad (19)$$

where  $t$  is the interparticle arrival time (Heinlein and Fritsching 2006). The interparticle arrival time analysis is conducted for narrow classes of particles of comparable sizes which are expected to have the same behaviour (Edwards and Marx 1995b). The study gives some information on preferential clustering for particular classes of particle sizes. In hydraulic jumps, the interparticle arrival time data analyses tended to show that bubble clustering occurred predominantly with small bubbles ( $< 0.5$  to  $1$  mm), while larger bubbles tended to be randomly distributed (Chanson 2007b, Gualtieri and Chanson 2010). In skimming flows on a stepped spillway, the results yielded some clustering across all particle sizes (Felder 2013). Figure 11 presents some experimental results for a skimming flow on a stepped spillway (configuration sketched in Fig. 9). The graphs show the data for two classes of bubble chords, in each presenting the Poisson distribution and the expected deviations from the Poisson distribution for the sample. The data set did not exhibit the characteristics of a random process because the experimental and theoretical distributions differ substantially in shape (Fig. 11).

In some non-stationary flows characterized with low-frequency oscillations, a traditional signal processing would yield some meaningless turbulence levels and turbulent properties. Examples include hydraulic jump flows and self-sustained instabilities in pooled stepped spillway flows. Felder and Chanson (2012) proposed a new signal processing method based upon a triple decomposition of the raw probe signals. The results highlighted that the largest contribution to the turbulent kinetic energy was caused by the slow, long-period fluctuations linked to the flow instabilities. The turbulence properties in terms of fast fluctuating signal component were qualitatively and quantitatively consistent with similar findings of steady stationary air–water flows. In periodic flows, the experiments may be performed over a large number of periods and the results are phase-averaged. A classical application is the air entrainment in breaking waves (Hwung *et al.* 1992, Cox and Shin 2003, Hoque and Aoki 2005b). In rapidly-varied unsteady flows, a different signal processing technique must be used. Practical applications encompass air entrainment in dam break waves and breaking tidal bores (Chanson 2004c, 2005, Docherty and Chanson 2010).

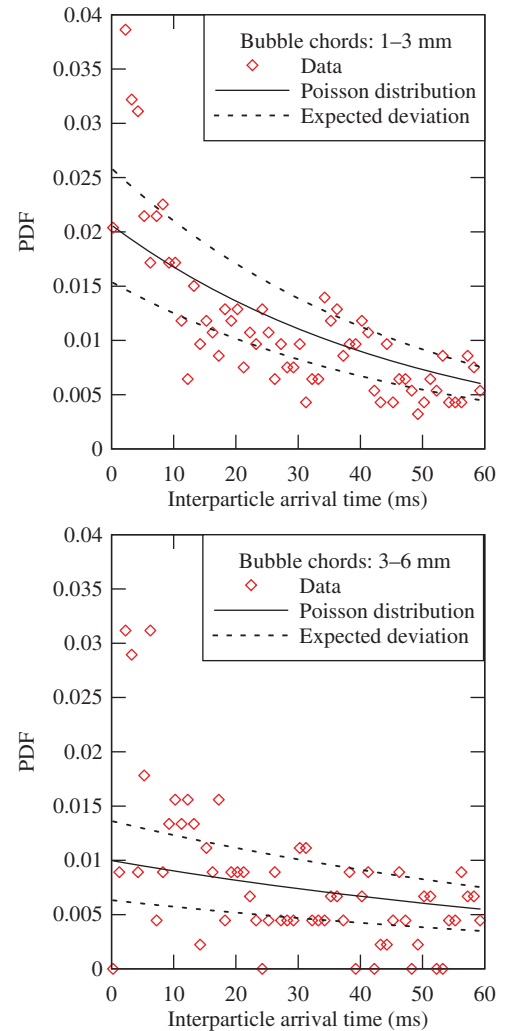


Figure 11 Distributions of interparticle arrival times in a skimming flow above a stepped spillway. Data: Felder and Chanson (2009),  $\theta = 21.8^\circ$ ,  $h = 0.05$  m,  $d_c/h = 2.39$ ,  $\rho_w q_w / \mu_w = 1.3 \times 10^5$ , step edge  $20$ ,  $y = 0.037$  m,  $C = 0.073$ ,  $F = 54$  Hz. Note that only two classes of bubbles are shown

## 5 The future of hydraulics of aerated flows

In turbulent free-surface flows, the deformation of the free-surface leads to some air bubble entrainment and droplet projections. The air–water flow becomes a compressible fluid with density  $\rho_w(1 - C) + \rho_a C \approx \rho_w(1 - C)$ . A number of experimental, numerical and theoretical advancements have been reported over the last two decades. The findings suggest that the physical modelling and laboratory experiments are essential tools to validate phenomenological, theoretical and numerical models (Hanratty *et al.* 2003). New developments in instrumentation and signal processing enable the measurements of a range of detailed turbulent gas–liquid flow properties under controlled flow conditions, which constitute a *sine qua non* requirement for clarifying flow physics and model validation (Roache 2009, Chanson and Lubin 2010).

What's next? At the microscopic scale, the theoretical equations are relatively straightforward, but for the sharp interface

definition (section 2). The interface tracking, the coupling of equations at the air–water interfaces and the correct implementation of the boundary conditions are “*not as easy as it may sound in engineering applications*” (Bombardelli 2012). These issues are especially true in aerated flows with uncontrolled air–water exchanges and local-averaged void fractions ranging from 0 to 100%. In the author’s opinion, the future research into aerated flow hydraulics should focus on (1) field measurements of high quality, (2) CFD modelling of aerated flows, (3) the development of signal processing software suites and (4) the hydraulics of aerated flows in conduits; the first point being the most critical.

### 5.1 Field measurements of high quality

The single most important drive of future research must come from new field measurements, performed *in situ* at the full-scale. Forty years on, the Aviemore dam spillway investigations (Keller 1972, Cain 1978) remain a key reference because there have been no follow-up detailed prototype measurements. Although a few further prototype observations were conducted, they are mostly qualitative like at the Dachashan dam spillway (Lin and Han 2001). The Aviemore dam spillway data sets must be urgently complemented with new field data collected at much larger systems. The flow conditions at the Aviemore dam spillway corresponded to the Reynolds numbers about  $2 \times 10^6$ , i.e. one to two orders of magnitude lower than the design flow conditions of large spillway systems. The previous discussions on dynamic similarity would suggest that the extrapolation of the Aviemore dam results could be subjected to some form of scale effects at larger Reynolds numbers. Simply, no prototype data means no definite validation of any kind of modelling!

A major challenge of many aerated flows at prototype scale is their three-phase nature that includes water, air and sediments, as illustrated in Fig. 12, with further illustrations in Figs. 1 and 2. In



Figure 12 Three-phase air–water–sediment flow at a prototype scale: Yang-Tse’-Kiang River (China) at Tiger Leaping Gorge in 2009 (Courtesy of Jean-Pierre Girardot)

many flood situations, the sediment load is large and thus turbulent modulation in sediment-laden flows cannot be neglected (Jha and Bombardelli 2009). Yet, no study was undertaken, to date, in three-phase flow with high sediment and air content despite the high practical relevance.

### 5.2 CFD modelling of aerated flows

The hydraulics of aerated flows can greatly benefit from the insights provided by numerical simulations, and the last decade has seen the development of powerful numerical capabilities with direct applications into gas–liquid flows (Prosperetti and Tryggvason 2009). The CFD modelling may supplement the use of physical models and address the intrinsic limitations of experimental measurements. Despite some works are available (Gonzalez and Bombardelli 2005, Sousa *et al.* 2009, Lubin *et al.* 2009), most numerical studies of aerated flows are barely addressing the fundamental challenges of physical processes (Bombardelli 2012), while lacking solid validation and verification (Chanson and Lubin 2010). For example, most validations are conducted in terms of flow depth and depth-averaged velocity, sometimes including a limited comparison of void fraction and time-averaged velocity distributions. A proper validation of CFD modelling results should be, at the very least, based upon the distributions of void fractions, velocity, turbulence intensity and bubble-droplet chord sizes. It could further include the distributions of turbulent integral length and time scales, as well as the microscopic flow structure (clustering, interparticle distances). A drawback of current CFD methods (DNS, LES) is the computational resources required to complete a simulation and the level of information necessary to describe the system boundary conditions. Based upon a rough approach (Nezu and Nakagawa 1993), a model domain with a grid small enough to capture processes at the Kolmogorov scale ( $\sim 10^{-4} - 10^{-5}$  m) would require about  $10^{10}$  and  $10^{17}$  mesh points for a small plunging jet and a large spillway flow, respectively. Furthermore, the number of operations required for CFD modelling is proportional to the Reynolds number as  $\propto R^{9/4}$  for DNS and  $\propto R^{3/2}$  for LES (Reynolds 1990, Lesieur 1997). Current DNS and LES approaches are restricted to some investigations of turbulent processes in simple geometries with relatively low Reynolds numbers ( $\sim 10^5$  for DNS) (Prosperetti and Tryggvason 2009).

### 5.3 Development of signal processing software suites

Despite some recent developments in signal processing (see above), very few studies presented systematically detailed air–water turbulent flow properties, with a broad spectrum of turbulent air–water parameters suitable for proper CFD modelling validation. A restriction may be the limited outputs of commercial software packages available with off-the-shelf instrumentation. It is also acknowledged that the data processing may be computationally challenging for samples recorded at high frequency for long durations. The development of open-source software suites

and their diffusion among the research community may assist with a more rigorous data outputs, hopefully with enhanced data quality. A standardization of data acquisition systems and binary format outputs might be a first requirement to implement such an approach together with a standardized protocol.

#### 5.4 Hydraulics of aerated flows in conduits

Current research into aerated flows, including the present contribution, focused on free-surface flows with unlimited and uncontrolled air supply. Aerated flows in closed conduits constitute a difficult topic because of some additional constraints (Falvey 1980, Ervine 1998). For example, the interactions between the air boundary layers above the flow and at the roof may affect the air entrainment processes (Ervine 1998, Speerli 1999); the compressibility effects and the supersonic gas–liquid flow conditions must be also taken into account (Cain 1978, Chanson 2004e). The available literature is limited, and sometimes provides contradicting results. Altogether, the hydraulics of aerated flow in closed conduits is a whole research topic in its own.

#### 5.5 Concluding remarks

“Turbulence and multiphase flows are two of the most challenging topics in fluid mechanics and when combined they pose a formidable challenge” (Balachandar and Eaton 2010). This is especially true for aerated flows in hydraulic engineering, with high-Reynolds numbers and uncontrolled self-aeration. There remain some critical issues with the validity of extrapolation of physical model results to prototype flow conditions, as well as with the validity of numerical results calibrated with and tested against small-scale laboratory data. A number of recent results demonstrated further that the notion of scale effects is closely linked with the selection of some characteristic turbulent flow property(ies), and true dynamic similarity might not be achieved unless at full scale in some cases (Chanson 2009).

Hydraulic engineering professionals and researchers must comprehend that the effects of flow aeration are not solely restricted to flow bulking and re-oxygenation. Further impacts include turbulence modulation, ranging from drag reduction on smooth and stepped chute spillways and turbulent kinetic energy enhancement in hydraulic jumps and breaking waves. The advanced understanding of the physical processes at the millimetre- and micro-scales is critical to any future progress.

The hydraulic research community must 惩前毖后 (learn from past mistakes to avoid future ones) and anyone should acknowledge that *ex nihilo nihil fit* (nothing comes from nothing). Let be no *qui pro quo* (misunderstanding)! A major research drive into the aerated flow hydraulics is required. The contribution of hydraulic engineers to air–water turbulent flow research has been relatively modest over the last 30 years, after some leading contributions during the 1930s to 1970s (Chanson 2007d). A comparison of developments in multiphase flow research and aerated flow hydraulic research suggests that there is a lack of

interactions between hydraulic engineering and multiphase flow experts. Less than five hydraulic research groups have regularly contributed to the prestigious *International Journal of Multiphase Flow* (Elsevier, 2011 Impact Factor = 2.23) for the last 20 years. For the same period (1992–2012), only 14 articles of this journal (out of 1866 published articles) cited contributions published by the *IAHR Journal of Hydraulic Research* or *ASCE Journal of Hydraulic Engineering*. The 2007 and 2010 editions of the International Conference on Multiphase Flow series attracted 750 and 1100 participants, respectively, with the participation of only two *IAHR* individuals. The hydraulic engineering field will continue to lag further and further behind the world expertise in gas–liquid flows and aerated flow fluid dynamics, with adverse consequences on the engineering designs with aerated flows, unless researchers and professionals are committed to major advancements in aerated flow research scholarship and cross-discipline collaboration.

#### Acknowledgements

The author thanks his research students (past and present) and collaborators for their inputs and contributions. This manuscript would not have been possible without their various contributions. The author also acknowledges some helpful exchanges with Professor F.A. Bombardelli (UC Davis) and Professor J. Matos (IST Lisbon). The author also thanks the JHR Editor Professor V. Nikora for his encouragements. The financial support of the Australian Research Council is acknowledged (Grants ARC DP0878922 & DP120100481).

#### Notation

$C$	= average void fraction (–)
$c$	= instantaneous void fraction: $c = 0$ in water and $c = 1$ in air (–)
$d$	= water depth or jet diameter (m)
$d_{ab}$	= bubble size (m)
$d_c$	= critical flow depth (m)
$d_o$	= inflow depth (m)
$F$	= bubble count rate (Hz)
$F_{\text{sampl}}$	= sampling frequency (Hz)
$F$	= Froude number (–)
$g$	= gravity acceleration ( $\text{m/s}^2$ )
$k_s$	= equivalent sand roughness height (m)
$L_{\text{int}}$	= turbulent integral length scale (m)
$MO$	= Morton number (–)
$N_c$	= number of bubble clusters per second (Hz)
$Q$	= volume discharge ( $\text{m}^3/\text{s}$ )
$q$	= discharge per unit width ( $\text{m}^2/\text{s}$ )
$R$	= Reynolds number (–)
$R_{xx}$	= normalized auto-correlation function (–)
$R_{xy}$	= normalized cross-correlation function (–)
$T$	= characteristic time lag for the cross-correlation function is maximum (s)
$Tu$	= turbulence intensity: $Tu = v'/V$ (–)

$T_{int}$	= turbulent integral time scale (s)
$T_{sampl}$	= sampling duration (–)
$T_{xx}$	= auto-correlation integral time scale (s)
$T_{xy}$	= cross-correlation integral time scale (s)
$t$	= interparticle arrival time (s)
$V$	= average velocity (m/s)
$v$	= instantaneous velocity (m/s)
$V_c$	= critical flow velocity (m/s)
$V_o$	= inflow velocity (m/s)
$V_{90}$	= characteristic velocity, where $C = 0.90$ (m/s)
$v'$	= turbulent velocity fluctuations (m/s)
$W$	= chute width (m)
$We$	= Weber number (–)
$Y_{90}$	= characteristic depth where $C = 0.90$ (m)
$x$	= longitudinal coordinate (m)
$y$	= vertical coordinate or distance normal to the invert (m)
$z$	= transverse coordinate (m)
$\Delta x$	= longitudinal separation between probe sensor (m)
$\Delta z$	= transverse separation between probe sensor (m)
$\mu$	= dynamic viscosity (Pa s)
$\nu$	= kinematic viscosity (m <sup>2</sup> /s)
$\theta$	= angle between chute invert and horizontal (–)
$\rho$	= density (kg/m <sup>3</sup> )
$\sigma$	= surface tension (N/m)
$\tau$	= shear stress (N/m <sup>2</sup> )
$\emptyset_{ip}$	= probe sensor size (m)

#### Indices

$a$	= air properties
$c$	= critical flow conditions
$o$	= inflow or nozzle flow conditions
$w$	= water properties
90	= characteristic flow conditions for $C = 0.90$

#### References

- AIAA (1998). *Guide for the verification and validation of computational fluid dynamics simulations*. American Institute of Aeronautics and Astronautics, Reston, VA, AIAA-G-077-1998.
- Arreguin, F., Echavez, G. (1986). Natural air entrainment in high velocity flows. Proc. Conf. *Advancements in aerodynamics, fluid mechanics and hydraulics*, 186–192, ASCE, Minneapolis, MN, June.
- Augier, P. (1996). Contribution à l'Etude et à la Modélisation Mécaniste-Statistique de la Distribution Spatiale des Apports d'Eau sous un Canon d'Irrigation: Application à la Caractérisation des Effets du Vent sur l'Uniformité d'Arrosage. *PhD. thesis*, ENGREF, Montpellier, France (in French).
- Babb, A.F., Aus, H.C. (1981). Measurements of air in flowing water. *J. Hydraulic Div.* 107(HY12), 1615–1630.
- Balachandar, S., Eaton, J.K. (2010). Turbulent disperse multi-phase flow. *Ann. Rev. Fluid Mech.* 42, 111–133.
- Barenblatt, G.I. (1996). *Scaling, self-similarity, and intermediate asymptotics*. Cambridge University Press, Cambridge.
- Bélanger, J.B. (1841). *Notes sur l'Hydraulique*. Ecole Royale des Ponts et Chaussées, Paris, France, session 1841–1842 (in French). Ecole Royal des Ponts et Chaussees.
- Boes, R.M., Hager, W.H. (2003). Two-phase flow characteristics of stepped spillways. *J. Hydraulic Eng.* 129(9), 661–670.
- Bogdevich, V.G., Evseev, A.R., Mlyuga, A.G., Migirenko, G.S. (1977). *Gas-saturation effect on near-wall turbulence characteristics*. Proc. 2nd Int. Conf. on Drag reduction, 25–37, BHRA Fluid Engineering, D2, Cambridge, UK.
- Bombardelli, F.A. (2012). Computational multi-phase fluid dynamics to address flows past hydraulic structures. Proc. 4th IAHR Intl. Symp. *Hydraulic structures*, APRH – Associação Portuguesa dos Recursos Hídricos [Portuguese water resources association], J. Matos, S. Pagliara, I. Meireles, eds. 9–11 February 2012, Porto, Portugal, 2, 19.
- Bombardelli, F., Chanson, H. (2009). Progress in the observation and modeling of turbulent multi-phase flows. *Env. Fluid Mech.* 9(2), 121–123.
- Bombardelli, F.A., Meireles, I., Matos, J. (2011). Laboratory measurements and multi-block numerical simulations of the mean flow and turbulence in the non-aerated skimming flow region of steep stepped spillways. *Env. Fluid Mech.* 11(3), 263–288.
- Borges, J.E., Pereira, N.H.C., Matos, J., Frizell, K.H. (2010). Performance of a combined three-hole conductivity probe for void fraction and velocity measurement in air-water flows. *Exp. Fluids* 48, 17–31.
- Bradshaw, P. (1971). *An introduction to turbulence and its measurement*. The Commonwealth and International Library of Science and Technology Engineering and Liberal Studies, Thermodynamics and Fluid Mechanics Division. Pergamon Press, Oxford.
- Brattberg, T., Chanson, H. (1998). Air entrapment and air bubble dispersion at two-dimensional plunging water jets. *Chem. Eng. Sci.* 53(24), 4113–4127. Errata: (1999). 54(12), 192.
- Brocchini, M., Peregrine, D.H. (2001a). The dynamics of strong turbulence at free surfaces. Part 1. Description. *J. Fluid Mech.* 449, 225–254.
- Brocchini, M., Peregrine, D.H. (2001b). The dynamics of strong turbulence at free surfaces. Part 2. Free-surface boundary conditions. *J. Fluid Mech.* 449, 255–290.
- Cain, P. (1978). Measurements within self-aerated flow on a large spillway. *PhD. thesis*, Ref. 78–18, Department of Civil Engineering, University of Canterbury, Christchurch, New Zealand.
- Cain, P., Wood, I.R. (1981a). Instrumentation for aerated flow on spillways. *J. Hydraulic Div.* 107(HY11), 1407–1424.
- Cain, P., Wood, I.R. (1981b). Measurements of self-aerated flow on a spillway. *J. Hydraulic Div.* 107(HY11), 1425–1444.
- Calzavarini, E., Berg, T.H. van der, Toschi, F., Lohse, D. (2008). Quantifying microbubble clustering in turbulent flow from single-point measurements. *Phys. Fluids* 20(4), 040702. doi: 10.1063/1.2911036.

- Carosi, G., Chanson, H. (2006). *Air-water time and length scales in skimming flows on a stepped spillway. Application to the spray characterisation*. Report No. CH59/06, Division of Civil Engineering, University of Queensland, Brisbane, Australia, July.
- Cartellier, A. (1992). Simultaneous void fraction measurement, bubble velocity, and size estimate using a single optical probe in gas-liquid two-phase flows. *Rev. Sci. Instrum.* 63(11), 5442–5453.
- Cartellier, A., Achard, J.L. (1991). Local phase detection probes in fluid/fluid two-phase flows. *Rev. Sci. Instrum.* 62(2), 279–303.
- Chang, K.A., Lim, H.J., Su, C.B. (2003). Fiber optic reflectometer for velocity and fraction ratio measurements in multiphase flows. *Rev. Sci. Instr.* 74(7), 3559–3565.
- Chanson, H. (1988). A study of air entrainment and aeration devices on a spillway model. *PhD. thesis*, Ref. 88-8, Department of Civil Engineering, University of Canterbury, New Zealand.
- Chanson, H. (1989). Flow downstream of an aerator. Aerator spacing. *J. Hydraulic Res.* 27(4), 519–536.
- Chanson, H. (1994). Drag reduction in open channel flow by aeration and suspended load. *J. Hydraulic Res.* 32(1), 87–101.
- Chanson, H. (1997a). *Air bubble entrainment in free-surface turbulent shear flows*. Academic Press, London, UK.
- Chanson, H. (1997b). Air bubble entrainment in open channels. Flow structure and bubble size distributions. *Int. J. Multiphase Flow* 23(1), 193–203.
- Chanson, H. (2002). Air-water flow measurements with intrusive phase-detection probes. Can we improve their interpretation? *J. Hydraulic Eng.* 128(3), 252–255.
- Chanson, H. (2004a). Drag reduction in skimming flow on stepped spillways by aeration. *J. Hydraulic Res.* 42(3), 316–322.
- Chanson, H. (2004b). *Environmental hydraulics of open channel flows*. Elsevier Butterworth-Heinemann, Oxford.
- Chanson, H. (2004c). Unsteady air-water flow measurements in sudden open channel flows. *Exp. Fluids* 37(6), 899–909.
- Chanson, H. (2004d). Hydraulics of rectangular dropshafts. *J. Irrig. Drain. Eng.* 130(6), 523–529.
- Chanson, H. (2004e). Compressibility of extra-high-velocity aerated flow: A discussion. *J. Hydraulic Res.* 42(2), 213–215.
- Chanson, H. (2005). Air-water and momentum exchanges in unsteady surging waters: An experimental study. *Exp. Thermal Fluid Sci.* 30(1), 37–47.
- Chanson, H. (2007a). Air entrainment processes in rectangular dropshafts at large flows. *J. Hydraulic Res.* 45(1), 42–53.
- Chanson, H. (2007b). Bubbly flow structure in hydraulic jump. *Eur. J. Mech. B/Fluids* 26(3), 367–384.
- Chanson, H. (2007c). Dynamic similarity and scale effects affecting air bubble entrainment in hydraulic jumps. Proc. 6th Int. Conf. *Multiphase flow ICMF 2007*, Leipzig, Germany, 11, M. Sommerfeld, ed., 9–13 July, Session 7, Paper S7\_Mon\_B\_S7\_Mon\_B\_3.
- Chanson, H. (2007d). Hydraulic engineering in the 21st century: Where to? *J. Hydraulic Res.* 45(3), 291–301.
- Chanson, H. (2008). Advective diffusion of air bubbles in turbulent water flows. In *Fluid mechanics of environmental interfaces*, C. Gualtieri and D.T. Mihailovic, eds. 163–196, Chapter 7. Taylor & Francis, Leiden, The Netherlands.
- Chanson, H. (2009). Turbulent air-water flows in hydraulic structures: Dynamic similarity and scale effects. *Env. Fluid Mech.* 9(2), 125–142.
- Chanson, H. (2010). Convective transport of air bubbles in strong hydraulic jumps. *Int. J. Multiphase Flow* 36(10), 798–814.
- Chanson, H. (2012). Momentum considerations in hydraulic jumps and bores. *J. Irrig. Drain. Eng.* 138(4), 382–385.
- Chanson, H., Aoki, S., Hoque, A. (2004). Physical modelling and similitude of air bubble entrainment at vertical circular plunging jets. *Chem. Eng. Sci.* 59(4), 747–754.
- Chanson, H., Aoki, S., Hoque, A. (2006). Bubble entrainment and dispersion in plunging jet flows: Freshwater versus seawater. *J. Coastal Res.* 22(3), 664–677.
- Chanson, H., Brattberg, T. (1998). Air entrainment by two-dimensional plunging jets: The impingement region and the very-near flow field. Proc. 1998 *ASME fluids eng. conf. FEDSM'98*, Washington, DC, 8, Paper FEDSM98-4806, 21–25 June.
- Chanson, H., Brattberg, T. (2000). Experimental study of the air-water shear flow in a hydraulic jump. *Int. J. Multiphase Flow* 26(4), 583–607.
- Chanson, H., Carosi, G. (2007a). Advanced post-processing and correlation analyses in high-velocity air-water flows. *Env. Fluid Mech.* 7(6), 495–508.
- Chanson, H., Carosi, G. (2007b). Turbulent time and length scale measurements in high-velocity open channel flows. *Exp. Fluids* 42(3), 385–401.
- Chanson, H., Chachereau, Y. (2013). Scale effects affecting two-phase flow properties in hydraulic jump with small inflow Froude number. *Exp. Thermal Fluid Sci.* 45, 234–242.
- Chanson, H., Felder, S. (2010). Turbulence measurements in air-water self-aerated flows: Basic analysis and results. Proc. 7th Int. Conf. *Multiphase flow ICMF 2010*, Tampa, FL, 11, Paper No. 10.3.4, 30 May–4 June.
- Chanson, H., Gonzalez, C.A. (2005). Physical modelling and scale effects of air-water flows on stepped spillways. *J. Zhejiang Univ. Sci.* 6A(3), 243–250.
- Chanson, H., Gualtieri, C. (2008). Similitude and scale effects of air entrainment in hydraulic jumps. *J. Hydraulic Res.* 46(1), 35–44.
- Chanson, H., Lee, J.F. (1997). Plunging jet characteristics of plunging breakers. *Coastal Eng.* 31(1–4), 125–141.
- Chanson, H., Lubin, P. (2010). Verification and validation of a computational fluid dynamics (cfd) model for air entrainment at spillway aerators. *Can. J. Civil Eng.* 37(1), 135–138.

- Chanson, H., Toombes, L. (2002). Air-water flows down stepped chutes: Turbulence and flow structure observations. *Int. J. Multiphase Flow* 28(11), 1737–1761.
- Coakley, D.B., Haldeman, P.M., Morgan, D.G., Nicolas, K.R., Penndorf, D.R., Wetzel, L.B., Weller, C.S. (2001). Electromagnetic scattering from large steady breaking waves. *Exp. Fluids* 30(5), 479–487.
- Cox, D.T., Shin, S. (2003). Laboratory measurements of void fraction and turbulence in the bore region of surf zone waves. *J. Eng. Mech.* 129(10), 1197–1205.
- Cummings, P.D. (1996). Aeration due to breaking waves. *PhD. thesis*, Department of Civil Engineering, University of Queensland, Australia.
- Cummings, P.D., Chanson, H. (1997a). Air entrainment in the developing flow region of plunging jets. Part 1. Theoretical development. *J. Fluids Eng.* 119(3), 597–602.
- Cummings, P.D., Chanson, H. (1997b). Air entrainment in the developing flow region of plunging jets. Part 2. Experimental. *J. Fluids Eng.* 119(3), 603–608.
- Docherty, N.J., Chanson, H. (2010). *Characterisation of unsteady turbulence in breaking tidal bores including the effects of bed roughness*. Hydraulic Model Report No. CH76/10, School of Civil Engineering, University of Queensland, Brisbane, Australia.
- Drew, D.A., Passman, S.L. (1998). Theory of multicomponent fluids. *Applied mathematical sciences*, Vol. 135, 308, J.E. Marsden, L. Sirovich, eds. Springer, New York, NY.
- Edwards, C.F., Marx, K.D. (1995a). Multipoint statistical structure of the ideal spray, Part I: Fundamental concepts and the realization density. *Atom. Spray* 5, 435–455.
- Edwards, C.F., Marx, K.D. (1995b). Multipoint statistical structure of the ideal spray, Part II: Evaluating steadiness using the interparticle time distribution. *Atom. Spray* 5, 435–455.
- Ehrenberger, R. (1926). Wasserbewegung in steilen Rinnen (Susstennen) mit besonderer Berücksichtigung der Selbstbelüftung. *Zeitschrift des Österreichischer Ingenieur und Architektverein*, No. 15/16 and 17/18 (in German).
- Elperin, T., Kleorin, N., Rogachevskii, I. (1996). Self-excitation of fluctuations of inertial particle concentration in turbulent fluid flow. *Phys. Rev. Lett.* 77(27), 5373–5376.
- Ervine, D.A. (1998). Air entrainment in hydraulic structures: A review. *Proc. Instn Civ. Engrs, Water, Maritime & Energy*, 130, 142–153.
- Ervine, D.A., Falvey, H.T. (1987). *Behaviour of turbulent water jets in the atmosphere and in plunge pools*. Proc. Instn Civ. Engrs., London, Part 2, 83, 295–314.
- Ervine, D.A., McKeogh, E.J., Elsayy, E.M. (1980). Effect of turbulence intensity on the rate of air entrainment by plunging water jets. *Proc. Instn. Civ. Engrs.*, Part 2, 69, 425–445.
- Falvey, H.T. (1980). *Air-water flow in hydraulic structures*. USBR Engrg. Monograph, No. 41, Denver, CO.
- Falvey, H.T. (1990). *Cavitation in chutes and spillways*. USBR Engrg. Monograph, No. 42, Denver, CO.
- Felder, S. (2013). Air-water flow properties on stepped spillways for embankment dams: Aeration, energy dissipation and turbulence on uniform, non-uniform and pooled stepped chutes. *PhD. thesis*, University of Queensland, School of Civil Engineering, Australia.
- Felder, S., Chanson, H. (2009). Turbulence, dynamic similarity and scale effects in high-velocity free-surface flows above a stepped chute. *Exp. Fluids* 47(1), 1–18.
- Felder, S., Chanson, H. (2012). *Air-water flow measurements in instationary free-surface flows: A triple decomposition technique*. Hydraulic Model Report No. CH85/12, School of Civil Engineering, University of Queensland, Brisbane, Australia.
- Foss, J., Panton, R., Yarin, A. (2007). Nondimensional representation of the boundary-value problem. In *Springer handbook of experimental fluid mechanics*, Part A, Chapter 2. C. Tropea, A. Yarin, J. Foss, eds. Springer, Heidelberg, Germany, 33–83.
- Führbötter, A. (1970). *Air entrainment and energy dissipation in breakers*. Proc. Int. Conf. Coastal Eng. ASCE, Washington DC, USA, 391–398.
- Gonzalez, C.A. (2005). An experimental study of free-surface aeration on embankment stepped chutes. *PhD. thesis*, Department of Civil Engineering, University of Queensland, Brisbane, Australia.
- Gonzalez, A., Bombardelli, F.A. (2005). *Two-phase-flow theoretical and numerical models for hydraulic jumps, including air entrainment*. Proc. 31st IAHR Biennial Congress, Seoul, South Korea.
- Gualtieri, C., Chanson, H. (2007). *Clustering process analysis in a large-size dropshaft and in a hydraulic jump*. Proc. 32nd IAHR Biennial Congress, Venice, Italy, G. Di Silvio, S. Lanzoni, eds. Topic C1.b (CD-ROM).
- Gualtieri, C., Chanson, H. (2010). Effect of Froude number on bubble clustering in a hydraulic jump. *J. Hydraulic Res.* 48(4), 504–508.
- Gulliver, J.S. (1990). *Introduction to air-water mass transfer*. Proc. 2nd Int. Symp. Gas transfer at water surfaces, air-water mass transfer, 1–7, S.C. Wilhelms, J.S. Gulliver, eds. ASCE Publications, Minneapolis, MN.
- Halbron, G., Durand, R., Cohen de Lara, G. (1953). *Air entrainment in steeply sloping flumes*. Proc. 5th IAHR Congress, IAHR-ASCE, Minneapolis, MN, 455–466.
- Hanratty, T.J., Theofanous, T., Delhay, J.M., Eaton, J., McLaughlin, J., Prosperetti, A., Sundaresan, S., Tryggvason, G. (2003). Workshop findings. *Int. J. Multiphase Flow* 29, 1047–1059.
- Heinlein, J., Fritsching, U. (2006). Droplet clustering in sprays. *Exp. Fluids* 40(3), 464–472.
- Henderson, F.M. (1966). *Open channel flow*. MacMillan Company, New York, NY.
- Héraud, D. (1966). Dispersion des Jets Liquides; Influence des Rugosités de Paroi. *PhD. thesis*, University Grenoble 1, France (in French).

- Hinze, J.O. (1955). Fundamentals of the hydrodynamic mechanism of splitting in dispersion processes. *J. AIChE* 1(3), 289–295.
- Hinze, J.O. (1975). *Turbulence*. ed. 2. McGraw-Hill Publications, New York, NY.
- Hoque, A., Aoki, S. (2005a). A quantitative analysis of energy dissipation among three typical air entrainment. *Env. Fluid Mech.* 5, 325–340.
- Hoque, A., Aoki, S.I. (2005b). Distributions of void fraction under breaking waves in the surf zone. *Ocean Eng.* 32(14–15), 1829–1840.
- Hoyt, J.W., Taylor, J.J. (1977). Waves on water jets. *J. Fluid Mech.* 83(Pt 1), 119–127.
- Hwung, H.H., Chyan, J.M., Chung, Y.C. (1992). *Energy dissipation and air bubbles mixing inside surfzone*. Proc. 23rd Int. Conf. Coastal eng., Venice, Italy, 308–321, Vol. 1, Chapter 22.
- Jevdjovich, V., Levin, L. (1953). *Entrainment of air in flowing water and technical problems connected with it*. Proc. 5th IAHR Congress, IAHR-ASCE, Minneapolis, MN, 439–454.
- Jha, S.K., Bombardelli, F.A. (2009). Two-phase modeling of turbulence in dilute sediment-laden, open channel flows. *Env. Fluid Mech.* 9, 237–266.
- Jones, O.C., Delhaye, J.M. (1976). Transient and statistical measurement techniques for two-phase flows: A critical review. *Int. J. Multiphase Flow* 3, 89–116.
- Keller, R.J. (1972). Field measurement of self-aerated high speed open channel flow. *PhD. thesis*, Department of Civil Engineering, University of Canterbury, New Zealand.
- Kim, S., Fu, X.Y., Wang, X., Ishii, M. (2000). Development of the miniaturized four-sensor conductivity probe and the signal processing scheme. *Int. J. Heat Mass Transfer* 43, 4101–4118.
- Kobus, H. (1984). Scale effects in modelling hydraulic structures. Proc. Int. Symp. *Scale effects in modelling hydraulic structures*, Esslingen, Germany.
- Lamb, P., Killen, J.M. (1950). *An electrical method for measuring air concentration in flowing air-water mixtures*. Technical Paper No. 2B, St Anthony Falls Laboratory, University of Minnesota, Minneapolis, MN.
- Lance, M., Bataille, J. (1991). Turbulence in the Liquid phase of a uniform bubbly air-water flow. *J. Fluid Mech.* 222, 95–118.
- Lesieur, M. (1997). *Turbulence in fluids*. ed. 3. Kluwer Academic Publications, Dordrecht, Germany.
- Lighthill, J. (1978). *Waves in fluids*. Cambridge University Press, Cambridge.
- Liggett, J.A. (1994). *Fluid mechanics*. McGraw-Hill, New York, NY.
- Lin, K., Han, L. (2001). *Stepped spillway for dachaoshan rec dam*. Proc. 29th IAHR Biennial Congress Special Seminar, Beijing, China, 88–93. P.H. Burgi, J. Gao, eds. SS2 Key Hydraulics Issues of Huge Water Projects.
- Liu, M., Rajaratnam, N., Zhu, D.Z. (2004). Turbulent structure of hydraulic jumps of low froude numbers. *J. Hydraulic Eng.* 130(6), 511–520.
- Lubin, P., Caltagirone, J.-P. (2009). Large eddy simulation of hydrodynamics generated by breaking waves. In *Advances in numerical simulations of nonlinear water waves*, 575–604, Vol. 11, Chapter 16. Q.W. Ma, ed., Series of Advances in Coastal and Ocean Engineering, World Scientific, Singapore.
- Lubin, P., Glockner, S., Chanson, H. (2009). *Numerical simulation of air entrainment and turbulence in a hydraulic jump*. Proc. Colloque SHF Modèles Physiques Hydrauliques: Outils Indispensables du XXIe Siècle? Société Hydrotechnique de France, Lyon, France, 24–25 November, 109–114.
- Ma, J., Oberai, A.A., Drew, D.A., Lahey Jr., Moraga, F.J. (2010). A quantitative sub-grid air entrainment model for bubbly flows – plunging jets. *Comput. Fluids* 39, 77–86.
- Madavan, N.K., Deutsch, S., Merkle, C.L. (1984). Reduction of turbulent skin friction by microbubbles. *Phys. Fluids* 27(2), 356–363.
- Marié, J.L. (1987). A simple analytical formulation for microbubble drag reduction. *PCH* 8(2), 213–220.
- Mehta, U.B. (1998). Credible computational fluid dynamics simulations. *AIAA J.* 36(5), 665–667.
- Murzyn, F., Chanson, H. (2008). Experimental assessment of scale effects affecting two-phase flow properties in hydraulic jumps. *Exp. Fluids* 45(3), 513–521.
- Neal, L.S., Bankoff, S.G. (1963). A high resolution resistivity probe for determination of local void properties in gas-liquid flows. *Am. Inst. Chem. J.* 9, 49–54.
- Neal, L.S., Bankoff, S.G. (1965). Local parameters in cocurrent mercury-nitrogen flow. *Am. Inst. Chem. J.* 11, 624–635.
- Nezu, I., Nakagawa, H. (1993). *Turbulence in open-channel flows*. IAHR Monograph, IAHR Fluid Mechanics Section, Balkema Publications, Rotterdam, The Netherlands.
- Novak, P., Cabelka, J. (1981). *Models in hydraulic engineering. Physical principles and design applications*. Pitman Publications, London, UK.
- Novak, P., Moffat, A.I.B., Nalluri, C., Narayanan, R. (2001). *Hydraulic structures*. ed. 2. Spon Press, London, UK.
- Noymer, P.D. (2000). The use of single-point measurements to characterise dynamic behaviours in spray. *Exp. Fluids* 29, 228–237.
- Peterka, A.J. (1953). *The effect of entrained air on cavitation pitting*. Joint Meeting Paper, IAHR/ASCE, Proc. Minnesota International Hydraulic Convention Minneapolis, MN, Aug. 1953, 507–518.
- Pfister, M., Hager, W.H. (2010). Chute aerators. I: Air transport characteristics. *J. Hydraulic Eng.* 136(6), 352–359.
- Prosperetti, A., Tryggvason, G. (2009). *Computational methods for multiphase flows*. Cambridge University Press, Cambridge.
- Rajaratnam, N. (1962). An experimental study of air entrainment characteristics of the hydraulic jump. *J. Inst. Eng. India* 42(7), 247–273.
- Rao, N.S.L., Kobus, H.E. (1971). *Characteristics of self-aerated free-surface flows. Water and waste water/current research and practice*, Vol. 10, Eric Schmidt Verlag, Berlin, Germany.

- Reif, T.H. (1978). *The effects of drag reducing polymers on the turbulence characteristics of the hydraulic jump*. Report EW-11-78, US Naval Academy, Annapolis, USA.
- Rensen, J., Luther, S., Lohse, D. (2005). The effect of bubbles on developed turbulence. *J. Fluid Mech.* 538, 153–187.
- Resch, F.J., Leutheusser, H.J. (1972). Le ressaut hydraulique: Mesure de turbulence dans la région diphasique. *J. La Houille Blanche* 4, 279–293 (in French).
- Reynolds, W.C. (1990). The potential and limitations of direct and large eddy simulations. In *Whither turbulence? Turbulence at the crossroads*, J.L. Lumley, ed. Springer, Lecture Notes in Physics, Vol. 357. Springer, Berlin, Germany, 313–343.
- Rizzi, A., Vos, J. (1998). Toward establishing credibility in computational fluid dynamics simulations. *AIAA J.* 36(5), 668–675.
- Roache, P.J. (1998). Verification of codes and calculations. *AIAA J.* 36(5), 697–702.
- Roache, P.J. (2009). Perspective: Validation—what does it mean? *J. Fluids Eng.* 131, 034503. doi: 10.1115/1.3077134.
- Rouse, H. (1937). Modern conceptions of the mechanics of turbulence. *Transactions*, 102, 463–543.
- Russell, S.O., Sheehan, G.J. (1974). Effect of entrained air on cavitation damage. *Can. J. Civil Eng.* 1, 97–107.
- Sagaut, P., Deck, S., Larcheveque, L. (2008). *Numerical simulation data: From validation to physical analysis*. Proc. 11ème Congrès Francophone de Techniques Laser CFTL 2008, Poitiers Futuroscope, France, 16–19 September, J.M. Most, L. David, F. Penot, L.E. Brizzi, eds. Invited plenary, 29–43.
- Sene, K.J. (1984). Aspects of bubbly two-phase flow. *PhD. thesis*, Trinity College, Cambridge.
- Sene, K.J., Hunt, J.C.R., Thomas, N.H. (1994). The role of coherent structures in bubble transport by turbulent shear flows. *J. Fluid Mech.* 259, 219–240.
- Sheng, Y.Y., Irons, G.A. (1991). A combined laser Doppler anemometry and electrical probe diagnostic for bubbly two-phase flow. *Int. J. Multiphase Flow* 17(5), 585–598.
- Sousa, V., Bombardelli, F.A., Chanson, H. (2009). *Numerical simulation of rectangular dropshafts using a volume-of-fluid (VoF) technique*. Proc. 33rd IAHR Biennial Congress, IAHR-ASCE-EWRI, Vancouver, Canada, 9–14 August, 7009–7016.
- Speerli, J. (1999). Strömungsprozesse in grundablassstollen. *PhD. thesis*, ETH-Zürich, VAW, Switzerland, Dissertation ETHZ No. 12583 (in German).
- Straub, L.G., Anderson, A.G. (1958). Experiments on self-aerated flow in open channels. *J. Hydraulic Div., Proc. ASCE.* 84(HY7), 1890.
- Straub, L.G., Lamb, O.P. (1956). Studies of Air Entrainment in Open-Channel Flows. *Transactions, ASCE*, 121, 30–44.
- Sun, S., Chanson, H. (2013). Characteristics of clustered particles in skimming flows on a stepped spillway. *Env. Fluid Mech.* 13(1), 73–87.
- Tennekes, H., Lumley, J.L. (1972). *A first course in turbulence*. The MIT Press, Cambridge, MA.
- Thandaveswara, B.S. (1974). Self aerated flow characteristics in developing zones and in hydraulic jumps. *PhD. thesis*, Department of Civil Engineering, Indian Institute of Science, Bangalore.
- Tooby, P.F., Wicks, G.L., Isaacs, J.D. (1977). The motion of a small sphere in a rotating velocity field: A possible mechanism for suspending particles in turbulence. *J. Geophys. Res.* 82(15), 2096–2100.
- Toombes, L. (2002). Experimental study of air-water flow properties on low-gradient stepped cascades. *PhD. thesis*, Department of Civil Engineering, University of Queensland, Brisbane, Australia.
- Toombes, L., Chanson, H. (2005). Air-water mass transfer on a stepped waterway. *J. Env. Eng.* 131(10), 1377–1386.
- Tryggvason, G., Scardovelli, R., Zaleski, S. (2011). *Direct numerical simulations of gas-liquid multiphase flows*. Cambridge University Press, Cambridge.
- Viollet, P.L., Chabard, J.P., Esposito, P., Laurence, D. (2002). Mécanique des Fluides Appliquée. Ecoulements Incompressibles dans les Circuits, Canaux et Rivières, autour des Structures et dans l'Environnement. *Presses des Ponts et Chaussées*, Paris, France, 2ème édition, 367 (in French).
- Volkart, P. (1980). The mechanism of air bubble entrainment in self-aerated flow. *Int. J. Multiphase Flow* 6, 411–423.
- Wang, L. (1998) Self-similarity of fluid flows. *Appl. Phys. Lett.* 73(10), 1329–1330.
- Wilhelms, S.C., Gulliver, J.S. (1989). *Self-aerating spillway flow*. Proc. Natl Conf. Hydraulic engineering, 881–533, M.A. Ports, ed. ASCE, New Orleans.
- Wood, I.R. (1983). Uniform region of self-aerated flow. *J. Hydraulic Eng.* 109(3), 447–461.
- Wood, I.R. (1985). Air water flows. Proc. 21st IAHR Biennial Congress, Melbourne, Australia, Keynote address, 18–29.
- Wood, I.R. (1991). Air entrainment in free-surface flows. *IAHR Hydraulic Structures Design Manual No. 4*, Hydraulic Design Considerations, Balkema Publications, Rotterdam, The Netherlands.
- Xi, R. (1988). Characteristics of self-aerated flow on steep chutes. Proc. Int. Symp. *Hydraulics for high dams*, 68–75. IAHR, Beijing, China.
- Zhang, G., Wang, H., Chanson, H. (2013). Turbulence and aeration in hydraulic jumps: Free-surface fluctuation and integral turbulent scale measurements. *Env. Fluid Mech.* 13(2), 189–204.